DISSERTATION

SPATIOTEMPORAL COMPLEXITY IN GINZBURG LANDAU EQUATIONS FOR ANISOTROPIC SYSTEMS

Submitted by

Yang Zou

Department of Mathematics

In partial fulfillment of the requirements

For the Degree of Doctor of Philosophy

Colorado State University

Fort Collins, Colorado

Summer 2012

Doctoral Committee:

Advisor: Iuliana Oprea
Co-Advisor: Gerhard Dangelmayr

Steven Fassnacht
Patrick Shipman

ABSTRACT

SPATIOTEMPORAL COMPLEXITY IN GINZBURG LANDAU EQUATIONS FOR ANISOTROPIC SYSTEMS

Nematic electroconvection is a paradigm example of pattern formation in anisotropic extended systems, where spatiotemporal chaos can arise at the onset of electroconvection. This dissertation is devoted to characterize and identify the instability mechanism generating the spatiotemporal complexity in the numerical simulations of a system of Ginzburg Landau equations, used to study the weakly nonlinear stability of waves' amplitudes of nematic electroconvective patterns. In particular, the following results pertaining to spatiotemporal complexity are discussed.

First, the simulated patterns are decomposed into central and noncentral spatial Fourier modes. The central modes form an invariant manifold, and the noncentral modes are transverse variables for this manifold. Simulations indicate that the bursts in the noncentral modes induce rapid switchings between a pair of symmetry-conjugated chaotic saddles in the central modes. Even though there are many degrees of freedom involved in these spatiotemporal chaotic patterns, a dimension reduction can be made by exploiting symmetries, leading to a small number of symmetry-adapted variables. A detailed investigation of the dynamics in the space of symmetry-adapted variables reveals that the spatiotemporal complexity is due to in-out intermittency caused by transverse instability of the invariant manifold.

Second, in order to understand the instability mechanism causing the switching dynamics in terms of a low dimensional model, a normal form for a Hopf bifurcation with a broken translation invariance posed in the space of the central modes

is introduced. Theoretical issues relating to symmetries and invariant subspaces are studied. A series of complex phenomena, including symmetry breaking and increasing, period doubling, chaos, transient chaos, crisis-induced intermittency and in-out intermitteny, is observed when an imperfection parameter measuring the strength of the symmetry breaking is varied. In certain parameter regimes bursts with certain magnitudes trigger rapid switchings between a pair of chaotic saddles. A new type of dynamics, identified as a new type of intermittency, is also discussed. Conclusions and further development are presented at the end of the dissertation.

TABLE OF CONTENTS

LIST OF FIGURES

Chapter 1

Introduction

1.1 Overview

We are surrounded by a diversity of natural patterns. Some patterns are stationary, such as roll patterns on a zebra, hexagons on a giraffe, straight or spiral patterns on a tree bark, a variety of intricate crystallized snowflake patterns, and so on. Other patterns vary with time, like the gaits of horses, or waves in the ocean. For example, when a horse trots, one diagonal pair of legs move in synchrony, while the other diagonal pair of legs move with a half-period phase shift. And when a horse paces or gallops, legs move in a different pattern [28]. Curiosity about the mechanism generating patterns motivates people to build up various mathematical models and numerous experiments, making it a gigantic topic with a long history of findings and conjectures, and a host of open questions. For example, Turing proposed a theory of Turing instability explaining formation of stationary patterns on animals' skins as a result of chemical interactions with different diffusion rates [55]. Physicists have investigated a number of fluid system experimentally, such as Rayleigh-Bénard convection or Taylor-Couette flow, to create orderly patterns, like rolls and hexagons, as well as disordered patterns [8].

Symmetry, or the lack of it, is an important feature to describe patterns. For example, 230 distinct symmetry classes are used to classify classical crystallography [28]. For steady state patterns, such as patterns on animals' skins, patterns can be described by spatial symmetry. For moving patterns from thermal convections and animal gaits, space-time symmetry can be used to characterize them. Symmetry is also a powerful tool to investigate the pattern-formation mechanism, and a great deal of information regarding dynamics can be deduced by symmetries of the dynamical system.

However, some patterns are disordered and chaotic in space and time. In this case it is extremely difficult to characterize patterns using symmetry alone. These patterns exhibit temporal chaos in small localized regions, and localized chaotic dynamics in one region interacts with others to generate spatial disorder, leading to spatiotemporal chaos (STC). STC, which was first studied in fluid systems, is among the most fascinating patterns for both theoreticians and experimentalists. In [47] a variety of STC examples from physics, chemistry, biology, neuroscience, and so on are described. Loosely speaking, STC can be considered as an extended version of low dimensional chaos, like dynamics in the Lorenz system for well chosen parameters, whose creation and characterization are well known [43]. However, due to the complexity of the coupling of many (possibly an infinite number of) spatial degrees of freedom of the pattern, which results in disorderly variation in the extended space, it is still an open question to find the instability mechanism generating the STC. There are several mathematical models exhibiting STC, like Swift-Hohenberg equations, coupled map on lattice, Ginzburg Landau equations, and so on, attracting many applied mathematicians and theoretical physicists to study their nonlinear dynamics [17].

The objective of this dissertation is to characterize the spatiotemporal complexity identified in the numerical study of a system of four globally coupled complex

Ginzburg Landau equations, modeling the dynamics of the oscillatory instability in anisotropic extended systems, such as the evolution of the amplitudes of two pairs of counterpropagating traveling waves in nematic electroconvection. The form of these Ginzburg Landau equations is inferred from translational and reflectional symmetries. The chaotic patterns from the system of Ginzburg Landau equations resemble the observed experimental STC in the nematic electroconvection [21, 42, 41].

In the following section of this Chapter we describe briefly two examples from fluid mechanics giving rise to pattern formation. One is the Rayleigh-Bénard convection, a prototype of pattern formation and STC in extended isotropic systems. The other example is the electroconvection in nematic liquid crystals, a prototype for an extended anisotropic system exhibiting complex dynamics. In Section 1.3 we introduce equivarient theory briefly which formalizes the concept of symmetry of patterns and the corresponding dynamical systems.

Mathematical models describing nonlinear dynamics in pattern formation begin in Chapter 2, where we review a reaction diffusion system modeling a transition from a uniform pattern to a nontrivial pattern in terms of a Hopf bifurcation in an extended anisotropic two-dimensional system. The nematic electroconvection example can be explained under such a mathematical framework. The oscillatory instability and anisotropy lead to two pairs of counterpropagating traveling wave solutions in four directions. Then we present a derivation of a system of four globally coupled Ginzburg Landau equations modeling the dynamics of these four waves' amplitudes based on symmetry considerations.

The main contributions of this dissertation, focusing on nonlinear dynamics of a system of four globally coupled Ginzburg Landau equations and its simplified versions, are presented in Chapters 3 and 4. We describe a STC scenario from the Ginzburg Landau system, and investigate its instability mechanism in Chapter 3. We identify an invariant manifold within the STC, and study the relation between the full STC

and dynamics in this manifold. A simple 2D map is provided to characterize the instability mechanism generating the STC.

In Chapter 4, motivated by features of the dynamics in the Ginzburg Landau system, we construct a low dimensional system to investigate how spatial modes with different orders interact and affect the dynamics on the invariant manifold introduced in Chapter 3. We study symmetries and invariant subspaces of this low dimensional system, as well as a series of novel complex dynamical behavior. Finally Chapter 5 summarizes the results, and suggests some future work and possible extensions of this investigation.

1.2 Pattern Formation

In this section we present a short introduction to two classical examples of pattern formation. One is the Rayleigh-Bénard convection, a canonical example in isotropic systems [8, 1, 17]. The other is nematic electroconvection, a paradigm for pattern formation for anisotropic system [26, 24, 25]. We use a system of four globally coupled complex Ginzburg Landau equations to study the second system in the following Chapters.

1.2.1 Rayleigh-Bénard Convection

Rayleigh-Bénard convection is one of the most comprehensively studied nonequilibrium fluid system in both experimental and theoretical aspects. The idealized experiment involves a pure fluid placed between two flat horizontal plates. Heat conductors for plates maintain the lower plate at a temperature ΔT above the upper plate temperature. Thus the fluid near the bottom plate expands and is less dense than the fluid near the top plate. Assuming the density ρ depends linearly on the temperature, the fluid from the bottom tends to raise up due to the buoyancy force. For

sufficiently small temperature difference the fluid remains at rest and heat is transported only by conduction from the bottom plate to the top one. Convection sets in when the temperature difference ΔT is strong enough to overcome the resistant effects due to viscosity, resulting in various kinds of Rayleigh-Bénard convective patterns. One control parameter in this setup, R, which is called the Rayleigh number, is the dimensionless ratio of the destabilizing buoyancy force to the stabilizing dissipative force,

$$R = \frac{\alpha g \Delta T d^3}{\kappa \nu},$$

where α is the thermal expansion coefficient for the fluid, g the acceleration of gravity, ν the kinematic viscosity, κ the thermal diffusivity and d the plate separation distance. There is another important dimensionless parameter, the Prandtl number, characterizing properties of viscosity and thermal conductivity,

$$\sigma = \nu/\kappa,$$

representing the ratio of the two damping mechanisms acting on the fluid.

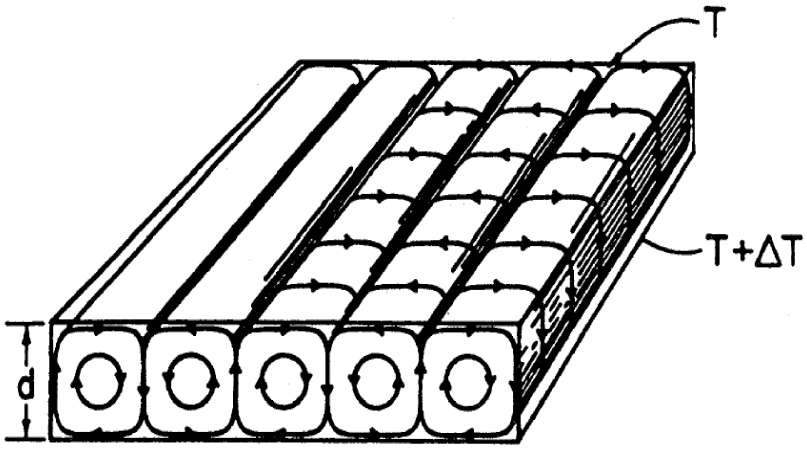

Figure 1.1: Schematic representation of the idealized roll pattern from Rayleigh-Bénard convection, from [17].

For Rayleigh number R slightly above a critical value, R_c, convective rolls are observed. The growth of the pattern is limited since convective flow transports part of the heat, therefore decreasing the temperature gradient and the buoyancy force. These nonlinear effects force the fluid to settle down to a certain level. Convective rolls are formed with diameters close to the separation distance d as illustrated in Figure 1.1. Other instabilities and subtle issues of wave number selections may result in superpositions of rolls forming hexagons or squares [1]. All these patterns are found in physical experiments above onset in different geometries, as shown in Figure 1.2.

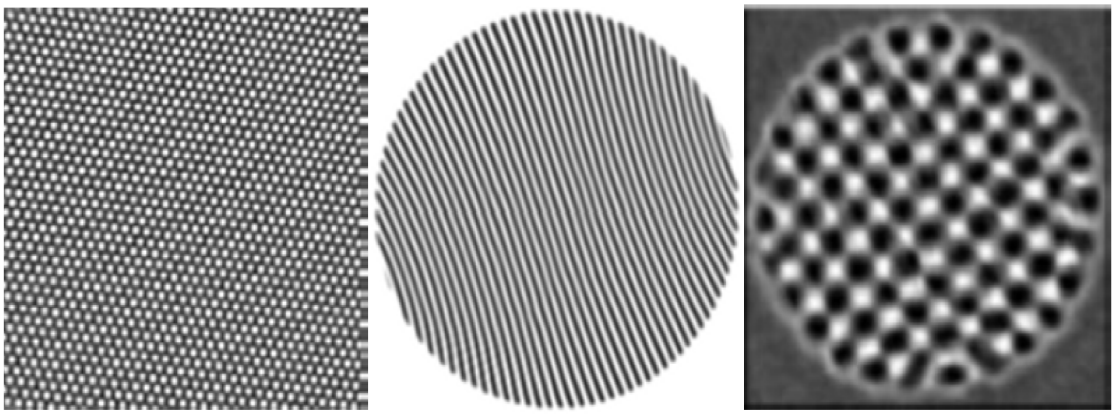

Figure 1.2: Hexagonal pattern, roll pattern, and square pattern from Rayleigh-Bénard convection in different geometries, from [1].

When the Rayleigh number R is increased further above the critical value R_c, the convection patterns may become chaotic in space and time, leading to STC. STC depends on a number of factors, such as the size of system, the Rayleigh number, the Prandtl number, and the geometry of the experimental devices [1, 17]. More degrees of freedom of STC come into play as the spatial extent increases. Here we present two examples of STC in Figure 1.3. Figure 1.3(a) represents complex patterns formed experimentally when a horizontal fluid is rotated about a vertical axis [32], exhibiting the coexistence of domain of rolls of more or less uniform orientation with other domains of a different orientation. Figure 1.3(b) shows another type of experimentally

observed STC, spiral-defect chaos, which consists of many small spirals, targets, and other defects in the roll structure [39]. The defects have a modest lifetime, and drift about irregularly. New defects are constantly created as old ones disappear.

(a) (b)

Figure 1.3: Two example of STC from Rayleigh-Bénard convection under different conditions. (a) from [32] and (b) from [39].

1.2.2 Nematic Electroconvection

Convection in nematic liquid crystals is a main paradigm for pattern formation in anisotropic systems [26, 24, 25]. For electroconvection, the charge carrying fluid is sandwiched between two electrode glass plates, across which an electric potential difference is applied. Unlike ordinary isotropic fluids, such as fluids in Rayleigh-Bénard convection, molecules of nematic liquid crystals are on average locally oriented along a preferred direction, called the director. When the amplitude and frequency of the external electrical field are above critical values, an electrohydrodynamic instability leads to a transition from the uniform state to a variety of patterns, including periodic patterns of convection rolls, localized structures, and STC. Anisotropy in nematic electroconvection results in four critical wave vectors with nonzero angles with respect to the director, allowing a unique reduced description through four amplitudes associated with two counterpropagating pairs of traveling waves in two oblique directions,

whose dynamics is governed by Ginzburg Landau amplitude equations. One pair of traveling waves in one oblique direction is referred to as zag rolls. The other is referred to as zig rolls.

Nematic electroconvection is a well-suited experimental system due to easy access to control parameters, i.e., the electrical conductivity and the amplitude and frequency of the applied electric potential difference. In [26, 24, 25] experimental observation of a variety of patterns is reported. We briefly describe two patterns here. One is an alternating-wave pattern provided in Figure 1.4. This pattern results from a superposition of zig and zag standing waves. One standing wave is one quarter of cycle out of phase with the other. The other example is STC from a different set of control parameters. Spatial demodulation is performed to generate amplitudes of zig and zag waves in Figure 1.5.

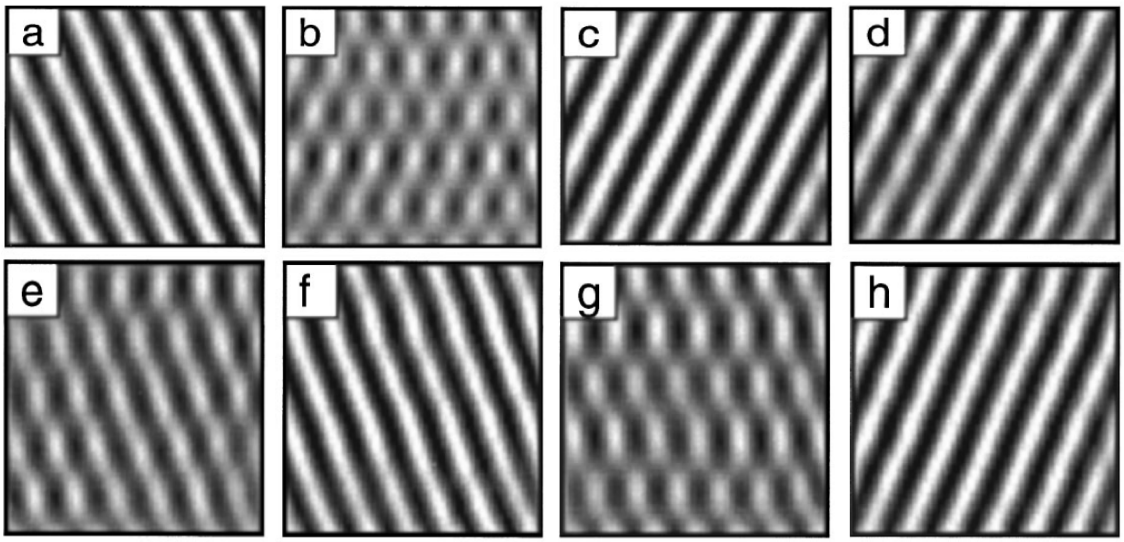

Figure 1.4: A time series of a pattern alternating between zig and zag rolls in nematic electroconvection, from [25].

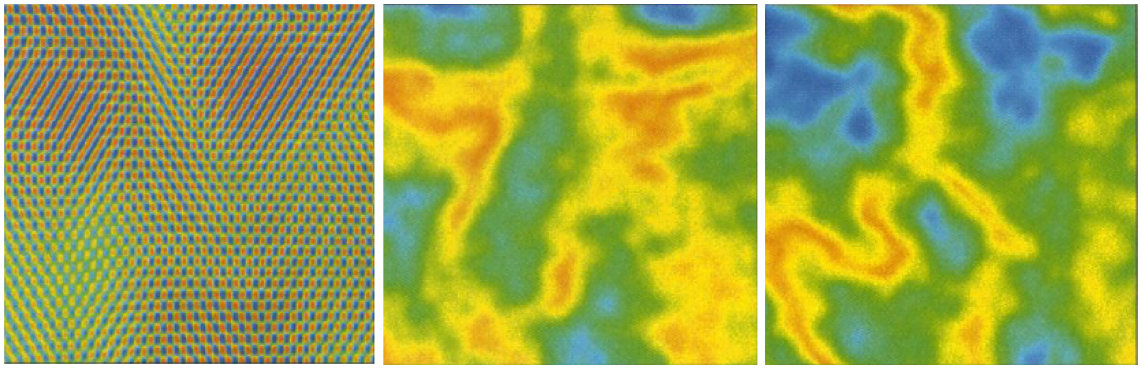

Figure 1.5: Left: an example of STC in nematic electroconvection. The maxima and minima are mapped to blue and red, respectively. Middle: the envelope of the zig rolls. Right: the envelope of the zag rolls, from [24].

1.3 Symmetry and Equivariance

Pattern formation involves the spontaneous breaking of a symmetry [17]. In order to formalize pattern formation from a symmetry point of view, we introduce in this section the concept of symmetry of a dynamical system and the concept of symmetry of a pattern, which is a solution of the governing equations of the dynamical system, in terms of equivariant theory [11, 28, 29].

Consider a dynamical system in $\mathbb{R}^n$,

$$\frac{dx}{dt} = f(x, \lambda), \tag{1.1}$$

which is defined by a smooth vector field $f : \mathbb{R}^n \times \mathbb{R}^r \to \mathbb{R}^n$ and depends on a set of parameters $\lambda \in \mathbb{R}^r$. Let γ be an $n \times n$ invertible matrix. We define a symmetry of a dynamical system as

Definition 1.2. *The invertible $n \times n$ matrix γ is a symmetry of (1.1) if for every solution $x(t) \in \mathbb{R}^n$ of (1.1), $\gamma x(t)$ is also a solution.*

Notice that if γ and δ are invertible matrices satisfying Definition 1.2, then both γ^{-1} and $\gamma\delta$ satisfy Definition 1.2. Therefore the set of symmetries of a dynamical system forms a group. We can extend the concept of a symmetry in Definition 1.2

from a concrete matrix to an abstract group element by representation theory. In the following of this dissertation, we call an element γ of a group Γ a symmetry of the dynamical system (1.1) if there is a representation T_γ acting on $\mathbb{R}^n$ such that the matrix T_γ satisfies the hypothesis of Definition 1.2. For ease of notation we write $\gamma x \equiv T_\gamma x$.

In application we need a more useful condition than Definition 1.2 to determine whether a group element γ is a symmetry of a dynamical system (1.1). Suppose $y(t) = \gamma x(t)$ is another solution of (1.1). Then

$$\dot{y}(t) = f(y(t)) = f(\gamma x(t)).$$

In addition,

$$\dot{y}(t) = \gamma \dot{x}(t) = \gamma f(x(t)).$$

Therefore,

$$f(\gamma x(t)) = \gamma f(x(t))$$

for all solutions $x(t)$ of (1.1). Since solutions exist for any arbitrary initial conditions, this is equivalent to

$$f(\gamma x) = \gamma f(x)$$

for all $x \in \mathbb{R}^n$, leading to the following condition of a symmetry group of a dynamical system.

Definition 1.3 (Γ-equivariant)**.** *Let Γ act on $\mathbb{R}^n$ and let $f : \mathbb{R}^n \times \mathbb{R}^r \to \mathbb{R}^n$ in (1.1). Then f is Γ-equivariant and Γ is a symmetry group for (1.1) if $f(\gamma x, \lambda) = \gamma f(x, \lambda)$ for all $\gamma \in \Gamma$, $x \in \mathbb{R}^n$.*

Next we formalize the notion of the symmetry of a pattern created in an equivariant dynamical system. In this finite dimensional setting a pattern is defined as an element x in the vector space $\mathbb{R}^n$ in which (1.1) is posed. A symmetry of the pattern

x is a group element σ from Γ in Definition 1.3, such that $\sigma x = x$. The set of all such σ's also preserves a group structure, the resulting group is known as the isotropy subgroup of x, i.e.,

Definition 1.4 (Isotropy subgroup)**.** *Let $v \in \mathbb{R}^n$. The isotropy subgroup of v is*

$$\Sigma_v = \{\gamma \in \Gamma : \gamma v = v\}.$$

Useful information about a pattern can be obtained from its isotropy subgroup. We can develop a technique for finding solutions with possible symmetries based on all isotropy subgroups of the system. First we need the following definition to classify different isotropy subgroups.

Definition 1.5 (Group orbit)**.** *Let $x \in \mathbb{R}^n$ and $\gamma \in \Gamma$. The group orbit of x is*

$$\Gamma x = \{\gamma x : \gamma \in \Gamma\}.$$

It is easy to see that

$$\Sigma_{\gamma x} = \gamma \Sigma_x \gamma^{-1},$$

thus the isotropy subgroup of γx is a conjugate subgroup of the isotropy subgroup of x. Because of this conjugacy property, we consider conjugate isotropy subgroups to be different expressions of the same symmetry, and classify patterns in terms of conjugacy classes of isotropy subgroups, by which we mean the set of all conjugates of a given isotropy subgroup. Containment defines relations between different conjugacy classes. To formalize this we define the following abstract structure:

Definition 1.6 (Conjugacy classes)**.** *Let $H = \{H_i\}$ and $K = \{K_j\}$ be two conjugacy classes of isotropy subgroups of Γ. Define a partial ordering $\leq$ on the set of such conjugacy classes by*

$$H \leq K \Leftrightarrow H_i \subseteq K_j$$

for some representatives H_i, K_j. The isotropy lattice of Γ in its action on $\mathbb{R}^n$ is the set of all conjugacy classes of isotropy subgroups, partially ordered by $\leq$.

The isotropy lattice classifies all possibilities for a pattern to break symmetry, which can be arranged in a hierarchy with the property that smaller isotropy subgroups correspond to breaking more symmetries.

Now we can develop a systematic method to search for patterns with any possible symmetries, using the structure of the isotropy lattice. For a given symmetry group in that structure, we can obtain a pattern with such symmetries using the following definition.

Definition 1.7 (Fixed-point subspace)**.** *Let $\Sigma \subseteq \Gamma$ be a subgroup. The fixed-point subspace of Σ is*

$$Fix(\Sigma) = \{v \in \mathbb{R}^n : \sigma v = v, \forall \sigma \in \Sigma\}.$$

We close this Chapter by the following theorem, which plays a vital role in the development of the theory of equivariant dynamics.

Theorem 1.8. *Let $f : \mathbb{R}^n \to \mathbb{R}^n$ be Γ-equivariant and let $\Sigma \subseteq \Gamma$ be a subgroup. Then*

$$f(Fix(\Sigma)) \subseteq Fix(\Sigma).$$

The above theorem implies that the dynamics of a pattern with isotropy subgroup Σ is restricted to the subspace $\mathrm{Fix}(\Sigma)$. Therefore to seek a pattern from a dynamical system with isotropy subgroup Σ, we restrict the search to the subspace $\mathrm{Fix}(\Sigma)$. Unless $\mathrm{Fix}(\Sigma)$ is the whole space $\mathbb{R}^n$, the searching problem is posed in a space of lower dimension, and ought to be simpler: the bigger Σ is, the smaller is the dimension of $\mathrm{Fix}(\Sigma)$. So we can start with the largest subgroups in the lattice of isotropy subgroups and work down the lattice systematically to determine patterns of the system with successively lower symmetries, i.e., smaller and smaller isotropy subgroups.

Chapter 2

Globally Coupled Complex Ginzburg Landau Equations

In this chapter we present mathematical models describing a transition from a uniform pattern to a nontrivial pattern and the dynamics of the resulting nontrivial pattern in anisotropic extended systems. Among physical extended anisotropic systems exhibiting STC, the electroconvection in nematic liquid crystals described in Section 1.2.2 is a paradigm example, allowing theoretical studies in terms of reduced amplitude or envelope equations of STC, which can arise directly at the onset of electroconvection [26, 24, 25]. In the following section we set up the mathematical framework of an anisotropic system of partial differential equations for patterns posed in a 3D layer that is infinitely extended in the horizontal directions. The system has two reflection invariances along two distinguished symmetry axes in the horizontal (x, y)-plane, and in addition we assume translation invariance in each of these two directions. In such a mathematical system pattern formation occurs if a spatiotemporally uniform solution undergoes a Hopf bifurcation, resulting in a spatiotemporal pattern with critical wave numbers located on both symmetry axes for the oblique case. The prototype example for this class of equations are the equations of the weak electrolyte model

(WEM) for electroconvection in nematic liquid crystals [53, 54]. Next we derive the amplitude equations of the spatiotemporal pattern, a system of four globally coupled complex Ginzburg Landau equations (GCCGLEs) [22], in Section 2.2. Simulations and analysis of the GCCGLEs are presented in the following chapters.

2.1 Hopf Bifurcation in Extended Anisotropic Systems

The phenomena of an initial, absolutely homogeneous state of a medium becoming inhomogeneous is always related to an exchange of stability [47]. In nonlinear dynamics such a transitions is defined as bifurcation, from which a phase portrait of a dynamical system changes its topological structure when a parameter is varied. We focus on a local bifurcation in this dissertation. For a continuous dynamical system, a local bifurcation occurs if the Jacobian matrix has an eigenvalue with zero real part. We call it a steady state bifurcation if such an eigenvalue is zero. If this eigenvalue is nonzero but purely imaginary, we call it a Hopf bifurcation, which leads to a spatiotemporal pattern. For global bifurcations, such as homoclinic and heteroclinic bifurcations, see [48] for an introduction.

In this chapter we build up the mathematical framework of a Hopf bifurcation in an extended anisotropic system with translation and reflection symmetries in the horizontal (x, y)-plane, from which the uniform trivial pattern loses stability, and a spatiotemporal pattern is formed. Consider the following reaction diffusion system,

$$\frac{\partial \mathbf{u}}{\partial t} = D_x \frac{\partial^2 \mathbf{u}}{\partial x^2} + D_y \frac{\partial^2 \mathbf{u}}{\partial y^2} + \mathbf{f}(\mathbf{u}, \mathcal{R}), \tag{2.1}$$

where D_x and D_y are diagonal diffusion matrices with positive entries. Due to the anisotropy, where the property of material is directionally dependent, D_x and D_y are

not equal. Assuming that the uniform trivial state $\mathbf{u}(\mathcal{R}) = \mathbf{0}$ is a solution of all values of the control parameter $\mathcal{R}$, $\mathbf{f}(\mathbf{0}, \mathcal{R})$ must be satisfied.

A standard linear stability analysis for the uniform trivial pattern can be applied to investigate how a spatiotemporal pattern is generated. We compute the linearized system of (2.1) as

$$\frac{\partial \mathbf{u}}{\partial t} = D_x \frac{\partial^2 \mathbf{u}}{\partial x^2} + D_y \frac{\partial^2 \mathbf{u}}{\partial y^2} + M(\mathcal{R})\mathbf{u}, \tag{2.2}$$

where $M(\mathcal{R}) = d_{\mathbf{u}}\mathbf{f}(\mathbf{0}, \mathcal{R})$ is the Jacobian matrix of $\mathbf{f}(\mathbf{u}, \mathcal{R})$. The spatiotemporal periodic form $\mathbf{u} = e^{\Sigma t} e^{i(px+qy)}\mathbf{U}$, where (p, q) is the wave vector and $\mathbf{U}$ is the constant mode, is considered, due to the translation symmetry in (x, y). Substituting it into (2.2) leads to the following eigenvalue problem,

$$K(p^2, q^2, \mathcal{R})\mathbf{U} = \Sigma \mathbf{U},$$

where $K(p^2, q^2, \mathcal{R}) = -p^2 D_x - q^2 D_y + M(\mathcal{R})$.

The neutral stability surface is defined by the eigenvalues of K as the set of all points in the $(p, q, \mathcal{R})$-space, such that some eigenvalues of K are on the imaginary axis, but no eigenvalues have positive real parts. Let $\mathcal{R}_c$ be the minimal value on the neutral stability surface. Then the uniform state $\mathbf{u} = \mathbf{0}$ becomes unstable for $\mathcal{R} > \mathcal{R}_c$. Here we focus on the scenario where $K_c = K(p^2, q^2, \mathcal{R}_c)$ has a pair of simple imaginary eigenvalues $\sigma(p^2, q^2, \mathcal{R}_c) = \pm i\omega_c$, and all other eigenvalues with negative real parts, in some neighborhood of $(p^2, q^2, \mathcal{R}_c)$, which corresponds to a Hopf bifurcation. Then $\omega_c > 0$ is the critical temporal frequency. Due to anisotropy and reflection symmetries along x-axis and y-axis, certain critical wave vectors $(\pm p_c, \pm q_c)$ are generated at isolated points $(\pm p_c, \pm q_c, \mathcal{R}_c)$ on the neutral stability surface, and the corresponding spatiotemporal patterns gain stability and replace the uniform state. The graphic representation of the neutral stability surface is presented in Figure 2.1.

Here critical group velocities can be defined as

$$v_p = \frac{\partial}{\partial p}\text{Im } \sigma(p^2, q^2, \mathcal{R}_c)|_{(p_c^2, q_c^2)}, \quad v_q = \frac{\partial}{\partial q}\text{Im } \sigma(p^2, q^2, \mathcal{R}_c)|_{(p_c^2, q_c^2)}. \tag{2.3}$$

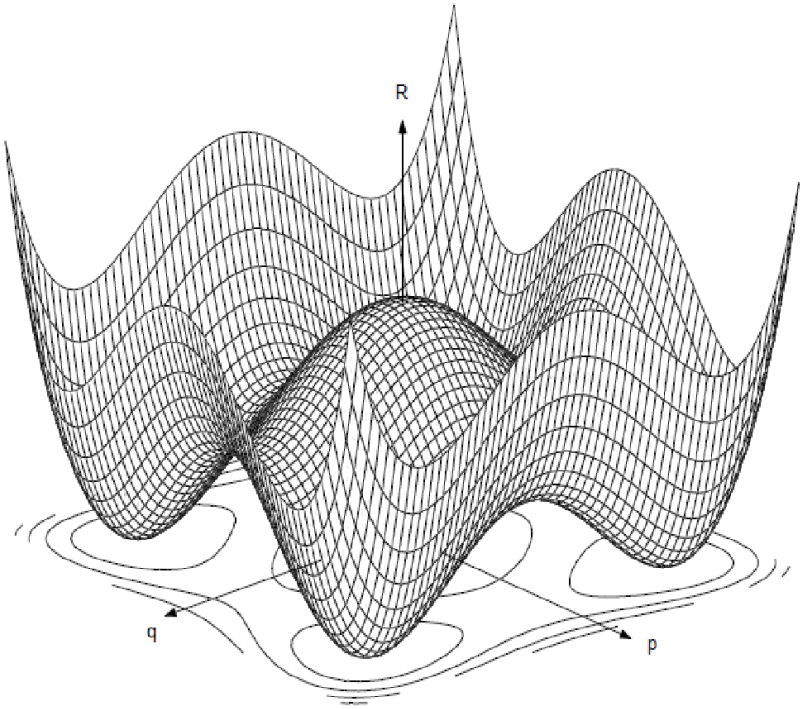

Figure 2.1: Neutral stability surface with four minima, from [58].

Next we can seek patterns with amplitudes in the form of small and slow temporal as well as spatial modulations of periodic functions, whose leading terms are the basic wave solutions of the linearized system (2.2). The pattern $\mathbf{u}$ is represented as

$$\begin{aligned} \mathbf{u} \;=\; & \big(\mathcal{A}_1 e^{i(p_c x + q_c y)}\mathbf{U}_1(z) + \mathcal{A}_2 e^{i(-p_c x + q_c y)}\mathbf{U}_2(z) + \\ & \mathcal{A}_3 e^{i(-p_c x - q_c y)}\mathbf{U}_3(z) + \mathcal{A}_4 e^{i(p_c x - q_c y)}\mathbf{U}_4(z)\big) e^{i\omega_c t} + \text{cc}, \end{aligned} \tag{2.4}$$

where $\mathcal{A}_1, \ldots, \mathcal{A}_4$ are small and slowly varying complex amplitudes, $(\pm p_c, \pm q_c)$ are the critical wave numbers, $\mathbf{U}_j(z)$ are vertical critical modes, and cc refers to the com-

plex conjugate expression. Patterns in extended anisotropic systems, such as complex nematic electroconvective patterns in Section 1.2.2 [26, 24, 25], can be analyzed under the framework of (2.4). For example, authors in [19] extracted the slowly varying envelopes from the space-time experiment data of the pattern using a four-wave demodulation based on representation (2.4), and diagnosed and characterized STC. Notice that (2.4) excludes some classic STC examples in isotropic systems, such as Rayleigh-Benard convection, because isotropy results in a full circle of critical wave vectors, making the representation through a finite set of plane-wave amplitudes impossible. In this dissertation we consider the case where $p_c > 0$ and $q_c > 0$, i.e., two pairs of counterpropagating traveling wave solutions in two oblique directions. In (2.4), $\mathcal{A}_1$ and $\mathcal{A}_3$ are amplitudes of plane waves traveling in the directions $-(p_c, q_c)$ and (p_c, q_c) ('zig-waves'), and $\mathcal{A}_2$ and $\mathcal{A}_4$ are amplitudes of plane waves traveling in the directions $(p_c, -q_c)$ and $(p_c, -q_c)$ ('zag-waves'), respectively. Analysis of the pattern $\mathbf{u}$ is equivalent to analysis of the dynamics of amplitude equations.

2.2 Derivation of the Globally Coupled Complex Ginzburg Landau Equations

The complex Ginzburg-Landau equation is one of the most popular nonlinear equations in the theory of pattern formation. Authors in [2] gave a review of various STC in Ginzburg-Landau, such as phase turbulence and defect chaos. Models using Ginzburg-Landau equations include pattern formation in 2D chemical reactor where an autocatalytic reaction takes places, the dynamics of excitations in nerve membranes, the field evolution in nonlinear optical resonators, structures in fluid flows, and so on [47].

In this section we derive amplitude equations for $\mathcal{A}_j$, $1 \leq j \leq 4$, of the pattern $\mathbf{u}$ in (2.4), which is a system of four globally coupled complex Ginzburg-Landau equations

(GCCGLEs). Since the amplitudes are small and slowly varying in space and time, we require that

$$|\frac{\partial \mathcal{A}_j}{\partial t}| \ll |\mathcal{A}_j| \ll 1, \quad |\frac{\partial^2 \mathcal{A}_j}{\partial x^2}| \ll |\frac{\partial \mathcal{A}_j}{\partial x}| \ll |\mathcal{A}_j|, \quad |\mathcal{R} - \mathcal{R}_c| \ll 1.$$

Then the weakly nonlinear analysis, an expansion in terms of the order parameter, can be applied to derive amplitude equations [23, 21].

In our case the system (2.1) has symmetries under time and space arbitrary translations

$$t \to t + t_0, \quad x \to x + x_0, \quad y \to y + y_0,$$

and two reflections

$$x \to -x, \quad y \to -y.$$

When applying the above operations to the pattern (2.4), we obtain the following symmetry actions on amplitudes $\mathcal{A}_j$, $1 \le j \le 4$,

$$\begin{aligned}
t \to t + t_0: \quad & (\mathcal{A}_1, \mathcal{A}_2, \mathcal{A}_3, \mathcal{A}_4) \;\to\; e^{i\omega_c t_0}(\mathcal{A}_1, \mathcal{A}_2, \mathcal{A}_3, \mathcal{A}_4), \\
x \to x + x_0: \quad & (\mathcal{A}_1, \mathcal{A}_2, \mathcal{A}_3, \mathcal{A}_4) \;\to\; (e^{ip_c x_0}\mathcal{A}_1, e^{-ip_c x_0}\mathcal{A}_2, e^{-ip_c x_0}\mathcal{A}_3, e^{ip_c x_0}\mathcal{A}_4), \\
y \to y + y_0: \quad & (\mathcal{A}_1, \mathcal{A}_2, \mathcal{A}_3, \mathcal{A}_4) \;\to\; (e^{iq_c y_0}\mathcal{A}_1, e^{iq_c y_0}\mathcal{A}_2, e^{-iq_c y_0}\mathcal{A}_3, e^{-iq_c y_0}\mathcal{A}_4), \\
x \to -x: \quad & (\mathcal{A}_1, \mathcal{A}_2, \mathcal{A}_3, \mathcal{A}_4) \;\to\; (\mathcal{A}_2, \mathcal{A}_1, \mathcal{A}_4, \mathcal{A}_3), \\
y \to -y: \quad & (\mathcal{A}_1, \mathcal{A}_2, \mathcal{A}_3, \mathcal{A}_4) \;\to\; (\mathcal{A}_4, \mathcal{A}_3, \mathcal{A}_2, \mathcal{A}_1).
\end{aligned} \tag{2.5}$$

We restrict the evolution of the amplitude equations

$$\partial \mathcal{A}_j / \partial t = \mathcal{F}_j(\partial_x, \partial_y, \mathcal{A}_1, \ldots, \mathcal{A}_4), \quad \text{for } 1 \le j \le 4,$$

to be invariant under symmetry operations in (2.5), therefore the general form of expansion of the right hand side, up to third order in $(\partial_x, \partial_y, \mathcal{A}_1, \ldots, \mathcal{A}_4)$, and second

order in $(\mathcal{R}-\mathcal{R}_c, \mathcal{A}_j)$, becomes

$$\frac{\partial \mathcal{A}_1}{\partial t} - v_p \frac{\partial \mathcal{A}_1}{\partial x} - v_q \frac{\partial \mathcal{A}_1}{\partial y} = (a(\mathcal{R}-\mathcal{R}_c) + \tilde{\mathcal{D}}(\partial_x, \partial_y) + \sum_{j=1}^{4} a_j |\mathcal{A}_j|^2)\mathcal{A}_1 + a_5 \mathcal{A}_2 \bar{\mathcal{A}}_3 \mathcal{A}_4 + \text{h.o.t.}, \tag{2.6}$$

where $\tilde{\mathcal{D}}(\partial_x, \partial_y)$ is the second-order differential operator

$$\tilde{\mathcal{D}}(\partial_x, \partial_y) = d_{pp}\partial_x^2 + 2d_{pq}\partial_x\partial_y + d_{qq}\partial_y^2,$$

and a, a_j, $1 \le j \le 5$ are complex coefficients, computed from a third-order Taylor expansion of (2.1). Derivation of $\mathcal{A}_j$, $2 \le j \le 4$, follows from reflection operators in (2.5). For example, we derive the equation of $\mathcal{A}_2$ by applying x-reflection symmetry, i.e., we change x to $-x$, and switch $\mathcal{A}_1$ with $\mathcal{A}_2$, and $\mathcal{A}_3$ with $\mathcal{A}_4$ in the equation (2.6).

Assuming that group velocities v_p and v_q in (2.3) cannot be treated as small parameters, we introduce slow wave variables

$$X_\pm = \epsilon(t \pm x/v_p), \qquad Y_\pm = \epsilon(t \pm y/v_q), \tag{2.7}$$

the superslow time $T = \epsilon^2 t$, and coefficient $a_0 = a(\mathcal{R}-\mathcal{R}_c)/\epsilon^2$, where $0 < \epsilon \ll 1$. The slow wave variables are not independent due to the relation

$$X_+ + X_- = Y_+ + Y_1. \tag{2.8}$$

We are now ready to set up the Ginzburg-Landau system for $O(1)$-amplitudes $\mathcal{A}_j$, $1 \le j \le 4$, which depend on slow time and space variables. The envelope $\mathcal{A}_1$ can be expanded in terms of order parameter ϵ as

$$\mathcal{A}_1 = \epsilon A_1(T, X_+, Y_+) + \epsilon^2 A_1^{(2)}(T, X_+, Y_+, X_-) + O(\epsilon^3), \tag{2.9}$$

$\mathcal{A}_j$, $2 \leq j \leq 4$, can be expanded in the similar way. Notice that three wave variables on which $A_1^{(2)}$ depends can be chosen arbitrarily because of the relation (2.8), and analogously for $A_2^{(2)}$, $A_3^{(2)}$, and $A_4^{(2)}$. When the expansion (2.9) is substituted into equation (2.6), at $O(\epsilon^3)$ we have

$$-2v_p \frac{\partial A_1^{(2)}}{\partial X_-} = \frac{\partial A_1}{\partial T} + (a_0 + \mathcal{D}(\partial_{X_+}, \partial_{Y_-}) + \sum_{j=1}^{4} a_j |A_j|^2) A_1 + a_5 A_2 \bar{A}_3 A_4, \qquad (2.10)$$

where

$$\mathcal{D}(\partial_{X_+}, \partial_{Y_-}) = D_{pp}\partial_{X_+}^2 + 2D_{pq}\partial_{X_+}\partial_{Y_+} + D_{qq}\partial_{Y_+}^2,$$

with

$$D_{pp} = d_{pp}/v_p^2, \quad D_{pq} = d_{pd}/(v_p v_q), \quad D_{qq} = d_{qq}/v_q^2,$$

is the rescaled differential operator. In order for the equation (2.10) to have a bounded solution, the average of the right hand side with respect to X_- must be zero, which leads to the following globally coupled Ginzburg Landau equation,

$$\begin{aligned} A_{1T} &= \{a_0 + \mathcal{D}(\partial_{X_+}, \partial_{Y_+}) + a_1|A_1|^2 + a_2 < |A_2(\xi, Y_+)|^2 > \\ &\quad + a_3 < |A_3(X_+ + \xi, Y_+ + \xi)|^2 > + a_4 < |A_4(X_+, \xi)|^2 > \} A_1 \\ &\quad + a_5 < A_2(X_+ + \xi, Y_+) \bar{A}_3(X_+ + \xi, Y_+ + \xi) A_4(X_+, Y_+ + \xi) >, \quad (2.11) \end{aligned}$$

where the brackets in (2.11) denote averages over ξ. The equations for A_2, A_3, A_4 follow from (2.11) by reflection symmetries. We set independent wave variables for A_j, $1 \leq j \leq 4$, as

$$A_1 = A_1(X_+, Y_+, T), \;\; A_2 = A_2(X_-, Y_+, T), \;\; A_3 = A_3(X_-, Y_-, T), \;\; A_4 = A_4(X_+, Y_-, T).$$

The equation (2.11) along with the corresponding equations for the other envelopes represent a system of globally coupled equations of the the Ginzburg Landau type.

Numerical simulation of this system, as well as the theoretical analysis, is presented in the following Chapter.

Chapter 3

Spatiotemporal Complexity in the Globally Coupled Complex Ginzburg Landau Equations

3.1 Introduction

In this Chapter we present a qualitative and quantitative analysis of a complex spatiotemporal pattern, which is a solution of four globally coupled complex Ginzburg Landau equations (GCCGLEs) (2.11) derived in Chapter 2. Unlike a low dimensional system, such as Lorenz equations [36] or logistic map [38], where different scenarios to chaos, such as period doubling cascade routes [27] or intermittency transitions [37, 45], have been established, in spatially extended systems the occurrence of complex spatiotemporal dynamics is only partially understood, and the problem of finding general approaches for the characterization of STC, as well as the identification of instability mechanisms generating it, is still open questions in nonlinear science.

A simulated complex spatiotemporal pattern from GCCGLEs by pseudo-spectral method is presented in Section 3.2. We decompose the pattern into central and

noncentral spatial Fourier modes using the Fourier-Galerkin expansion. The central modes form an invariant manifold, which is called the normal form and described in Section 3.3. Even though the chaotic pattern involves a lot of degrees of freedom, we reduce the dimension through exploiting the symmetries of the modes, leading to the dynamics of two symmetry-adapted variables in Section 3.4. By the end of this Chapter we identify and characterize the instability mechanism causing STC in terms of in-out intermittency by a 2D map.

3.2 Spatiotemporal Chaos

In this section we present a complex spatiotemporal pattern as a simulated solution of a system of GCCGLEs (2.11) from the previous Chapter. First we discuss the spectral method used in solving (2.11), then we describe the pseudo-spectral numerical scheme used to simulate (2.11).

Spectral methods can be applied to approximate solutions of partial differential equations (PDEs) as a linear combination of continuous functions which are generally nonzero over the whole domain of the solution. These continuous functions, called basis functions, are chosen based on the properties of the problem, such as smoothness or boundary conditions. The common choices include Fourier sinusoids or Chebyshev polynomials [52]. If Fourier sinusoids are chosen as basis functions, then the spectral method projects PDEs into the space spanned by the Fourier modes. The next task is to solve a system of ordinary differential equations (ODEs), time-dependent variables for the truncated Fourier modes, in the Fourier space. Spectral methods work very well for linear PDEs. However, for nonlinear PDEs, issues of spectral method come out due to the loss of the superposition principle for the solution from nonlinear terms.

The pseudospectral method, which has the same underlying principles as the spectral method regarding an orthonormal basis functions, can be applied to solve such

issues [58]. The collocation method is partially used in the pseudospectral method, where the solution is approximated by a linear combination of basis functions, but the coefficients are computed using a set of nodes in real space, called collocation points. Therefore nonlinear terms are evaluated in real space, instead of in Fourier space, and we can transform the result into Fourier space using a discrete Fourier transform, usually the Fast Fourier transform (FFT). By the end, a system of ODEs is derived and solved.

For the numerical simulation for the system of GCCGLEs (2.11) we use the following Fourier-Galerkin expansion,

$$A_j(X,Y,T) = \sum_{m=-M}^{M}\sum_{n=-N}^{N} a_{m,n}^{(j)}(T)e^{i(mrX+nsY)}, \quad 1 \le j \le 4, \tag{3.1}$$

with appropriately chosen spatial periods $(2\pi/r, 2\pi/s)$, see [21] for details. We drop here the subscripts $\pm$, since they just disappear after averages are taken. By putting (3.1) into (2.11) and projecting it in the Fourier space, we derive the following ODE system

$$\begin{aligned}
\frac{d}{dT}a_{m,n}^{(1)} &= [a_0 - (d_{20}p_m^2 + 2d_{11}p_m q_n + d_{02}q_n^2)]a_{m,n}^{(1)} \\
&\quad + a_1 \sum_u \sum_n \sum_s \sum_t a_{u,v}^{(1)} \bar{a}_{s,t}^{(1)} a_{m+s-u,n+t-v}^{(1)} \\
&\quad + a_2 \sum_u \sum_v \sum_t a_{u,v}^{(2)} \bar{a}_{u,t}^{(2)} a_{m,n+t-v}^{(1)} \\
&\quad + a_3 \sum_u \sum_v a_{u,v}^{(3)} \bar{a}_{u,v}^{(3)} a_{m,n}^{(1)} \\
&\quad + a_4 \sum_u \sum_v \sum_s a_{u,v}^{(4)} \bar{a}_{s,v}^{(4)} a_{m+s-u,n}^{(1)} \\
&\quad + a_5 \sum_u \sum_v a_{u,n}^{(2)} \bar{a}_{u,v}^{(3)} a_{m,v}^{(4)},
\end{aligned} \tag{3.2}$$

where $p_m = mp_c v_x/(\epsilon K_x)$, $q_n = nq_c v_y/(\epsilon K_y)$, and K_x and K_y are spatial periods in x and y directions, respectively [22]. Equations for $a_{m,n}^{(2)}(T)$, $a_{m,n}^{(3)}(T)$, $a_{m,n}^{(4)}(T)$ can

be derived from (3.2) based on symmetry considerations. To visualize a numerical solution as a spatiotemporal pattern, we associate with the A_j the function

$$\begin{aligned} u(t,x,y) &= \mathrm{Re}\{A_1(\epsilon^2 t, X_+, Y_+)e^{i(\omega_c t + p_c x + q_c y)} \\ &\quad + A_2(\epsilon^2 t, X_-, Y_+)e^{i(\omega_c t - p_c x + q_c y)} \\ &\quad + A_3(\epsilon^2 t, X_-, Y_-)e^{i(\omega_c t - p_c x - q_c y)} \\ &\quad + A_4(\epsilon^2 t, X_+, Y_-)e^{i(\omega_c t + p_c x - q_c y)}\}, \end{aligned} \tag{3.3}$$

with $X_\pm$ and $Y_\pm$ defined in (2.7). Notice that the pattern $u(t,x,y)$ in (3.3) is spatially periodic with periods $L_x = K_x 2\pi/p_c$ in x-direction, and $L_y = K_y 2\pi/q_c$ in y-direction.

For convolutions in the Fourier space, like $\sum_u \sum_n \sum_s \sum_t a^{(1)}_{u,v} \bar{a}^{(1)}_{s,t} a^{(1)}_{m+s-u,n+t-v}$ in (3.2), we can incorporate the FFT and inverse FFT into simulations to transform convolution terms between real and Fourier spaces. The convolutions, which corresponds to nested loops in simulation, can be transformed by inverse FFT to vectorwise multiplications. Then FFT can transform resulting terms from products back to Fourier space, and ODE solvers can be used to solve them. Therefore, the overall simulation time can be greatly reduced. The implementation of FFT and inverse FFT, as well as vectorization in Matlab, to reduce or eliminate the loops to improve the efficiency is discussed in detail in [58].

We have solved the differential equations for the $a^{(j)}_{m,n}(T)$ in (3.2) numerically for

random initial conditions using $M = N = 16$, with parameters

$$\begin{aligned}
a_0 &= 1, & a_1 &= -1 - 1.1806i, \\
a_2 &= -0.923 - 0.5538i, & a_3 &= -0.6442 + 1.3613i, \\
a_4 &= -0.2223 - 3.3025i, & a_5 &= -0.4647 - 0.2472i, \\
D_{11} &= 1 + 0.01i, & D_{12} &= 0.44 + 0.015i, \\
D_{22} &= 1 + 0.03i, & r &= 0.074, \\
s &= 0.076.
\end{aligned} \tag{3.4}$$

The envelopes of the resulting pattern from this simulation are depicted in Figure 3.1. Since all Y-modes (modes with $n \neq 0$) decay to zero, the envelopes eventually depend only on (X, T) ($X = X_+$ or X_-).

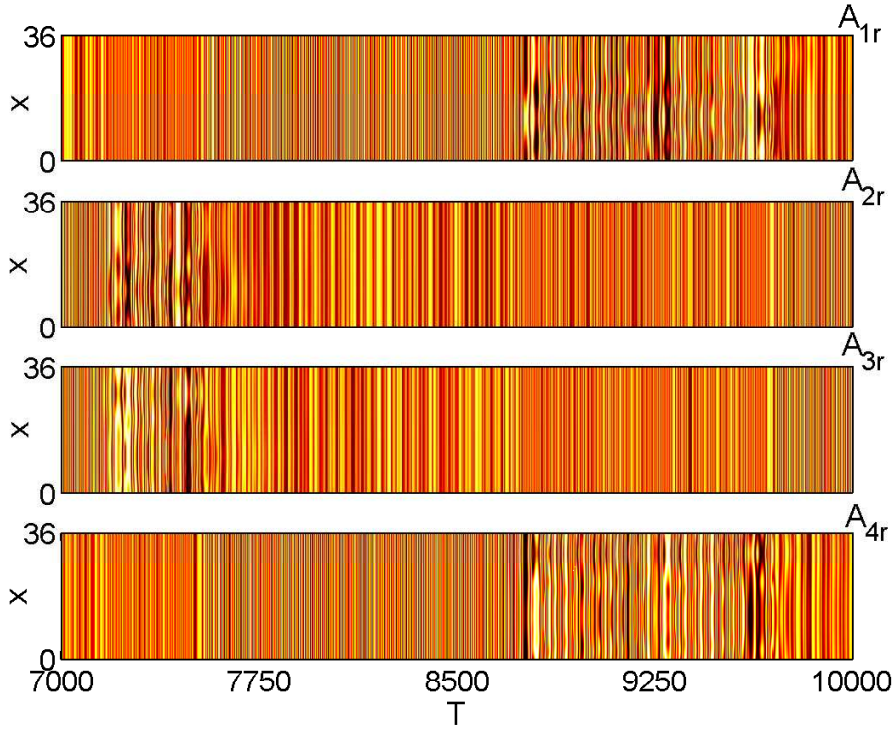

Figure 3.1: Color-coded plots of $A_{jr}(X, T)$ (36 space-points) for $7000 \leq T \leq 10000$ in Fourier-Galerkin simulation of the Ginzburg Landau system (2.11), with parameters given in (3.4). Since the Y-modes decay to zero, the A_j eventually are functions of (X, T) only.

The time series of the central modes (modes with $m = n = 0$) shown in Figure 3.2(a) indicate irregular rapid transitions ("switches") between symmetry-conjugated copies of two chaotic sets. Phase plane plots for zooms into time windows during which the trajectories reside in either of these sets are shown in the upper and lower panels of Figure 3.2(b). These plots indicate that the chaotic sets are symmetric with respect to x-reflection, i.e.

$$(A_1, A_2, A_3, A_4) \quad \rightarrow \quad (A_2, A_1, A_4, A_3). \tag{3.5}$$

The bursts exhibited by the time series of the first order X-modes (modes with $m = 1$ and $n = 0$) displayed in Figure 3.3 indicate that the switches are triggered when these modes get excited. The time series of the amplitudes of higher order noncentral X-modes (modes with $|m| > 1$ and $n = 0$) show similar bursting behavior and lead to the phases of non-uniform spatial behavior apparent in the plots of $A_{jr}(X, T)$ displayed in Figure 3.1. When all higher order modes in (3.1) are equal to zero, the central modes follow a normal form for a Hopf bifurcation with $\mathbb{O}(2) \times \mathbb{O}(2)$-symmetry [49, 57], which forms a low dimensional invariant submanifold from a big system. Six basic wave patterns are derived and analyzed in the following section. Noncentral modes, which are transverse variables, exhibit some form of intermittent behavior relative to the invariant subspace in Figure 3.3. The scenario of intermittency in Figure 3.3, which indicates in-out intermittency as described in [5, 12], is provided in detail in the Section 3.4.

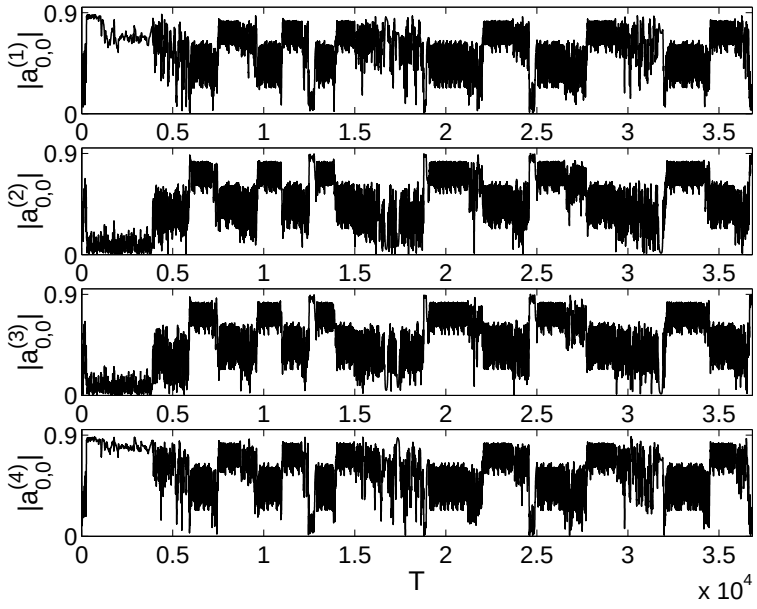

(a)

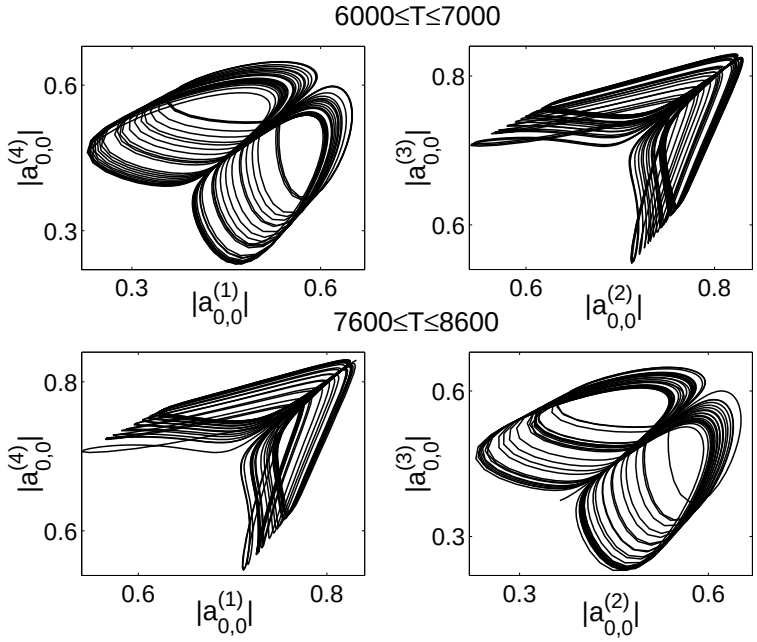

(b)

Figure 3.2: Fourier-Galerkin simulation of the Ginzburg Landau system (2.11) with parameters given in (3.4). (a): Time plots of the central modes. (b) Phase plane plots of the central modes for $6000 \leq T \leq 7000$ and $7600 \leq T \leq 8600$.

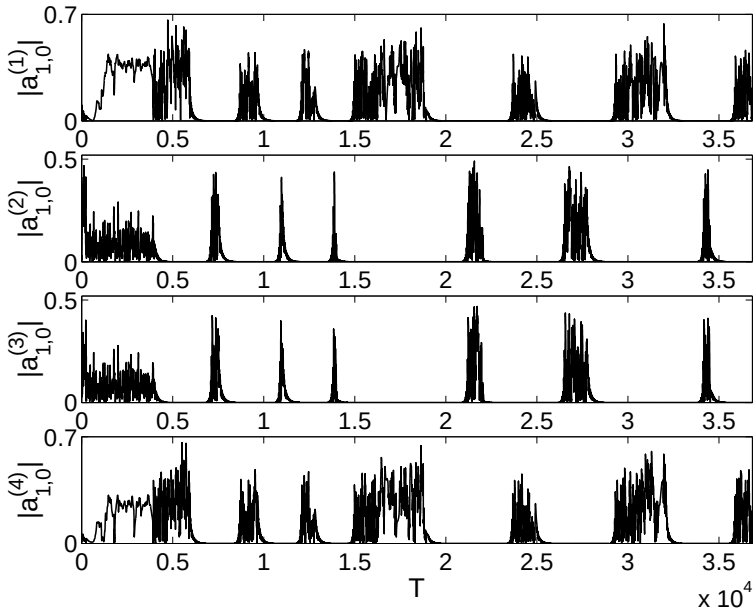

Figure 3.3: Time plots of first X-modes ($X = X_+$ or X_-) in Fourier-Galerkin simulation of the Ginzburg Landau system (2.11), with parameters given in (3.4). All Y-modes ($n \neq 0$) in (3.1) decay to zero.

3.3 An Invariant Manifold: Normal Form

3.3.1 Derivation of the Normal Form

Consider a spatially uniform and time-dependent pattern on the horizontal (x, y)-plane with $(2\pi/p_c, 2\pi/q_c)$-periodicity in (x, y), two reflection symmetries about x and y axises, and one overall phase symmetry imposed. The oscillatory instability leads to a Hopf bifurcation resulting in four traveling waves in four oblique direction. Denoting these four amplitudes by complex variables z_j, $1 \leq j \leq 4$, the dynamics of z_j in a neighborhood of the Hopf bifurcation point follows directly from the Ginzburg Landau system (2.11) when spatial variations in (2.11) are ignored, which is the

following Normal form for a Hopf bifurcation with $\mathbb{O}(2) \times \mathbb{O}(2)$-symmetry,

$$\begin{aligned}
\dot{z}_1 &= (a_0 + a_1|z_1|^2 + a_2|z_2|^2 + a_3|z_3|^2 + a_4|z_4|^2)z_1 + a_5 z_2 \overline{z}_3 z_4, \\
\dot{z}_2 &= (a_0 + a_1|z_2|^2 + a_2|z_1|^2 + a_3|z_4|^2 + a_4|z_3|^2)z_2 + a_5 z_1 z_3 \overline{z}_4, \\
\dot{z}_3 &= (a_0 + a_1|z_3|^2 + a_2|z_4|^2 + a_3|z_1|^2 + a_4|z_2|^2)z_3 + a_5 \overline{z}_1 z_2 z_4, \\
\dot{z}_4 &= (a_0 + a_1|z_4|^2 + a_2|z_3|^2 + a_3|z_2|^2 + a_4|z_1|^2)z_4 + a_5 z_1 \overline{z}_2 z_3,
\end{aligned} \tag{3.6}$$

where the dots represent the derivative d/dT with respect to a slow time $T = \epsilon^2 t$ (recall that ϵ^2 measures deviation of the bifurcation parameter from the critical value), and $a_0, a_1, \ldots, a_5$ are complex coefficients, same as coefficients in Ginzburg Landau equation (2.11). The system (3.6) is equivariant under the following actions of $\mathbb{O}(2) \times \mathbb{O}(2) \times \mathbb{S}^1$, which can be inferred by applying spatial translations and reflections and time translations to (2.4),

$$\begin{aligned}
T_t \quad & t \to t + t_0 : \ (z_1, z_2, z_3, z_4) \ \to \ e^{i\omega_c t_0}(z_1, z_2, z_3, z_4), \\
T_x \quad & x \to x + x_0 : \ (z_1, z_2, z_3, z_4) \ \to \ (e^{ip_c x_0} z_1, e^{-ip_c x_0} z_2, e^{-ip_c x_0} z_3, e^{ip_c x_0} z_4), \\
T_y \quad & y \to y + y_0 : \ (z_1, z_2, z_3, z_4) \ \to \ (e^{iq_c y_0} z_1, e^{iq_c y_0} z_2, e^{-iq_c y_0} z_3, e^{-iq_c y_0} z_4), \\
R_x \quad & x \to -x : \ (z_1, z_2, z_3, z_4) \ \to \ (z_2, z_1, z_4, z_3), \\
R_y \quad & y \to -y : \ (z_1, z_2, z_3, z_4) \ \to \ (z_4, z_3, z_2, z_1).
\end{aligned} \tag{3.7}$$

The Ginzburg Landau system (2.11) is an extension of the ODE normal form (3.6) and allows patterns with varying spatial periods, describing the dynamics in a spatially extended anisotropic system with many degrees of freedom. Notice that four central Fourier modes and zero noncentral Fourier modes in the expansion (3.1) form an invariant manifold, and the ODE normal form describes the dynamics of the system (3.2) restricting to the invariant manifold.

There is another way described in [49] to derive the normal form (3.6). If we consider amplitudes of the pattern (2.4) to be spatially uniform, equivariance with

respect to (3.7) leads to the dynamics of $\dot{z}_1 = g_1(z)$ with

$$g_1 = z_1 G + z_2 \bar{z}_3 z_4 H,$$

where

$$G \equiv G(|z_1|^2, |z_2|^2, |z_3|^2, |z_4|^2, z_1\bar{z}_2 z_3 \bar{z}_4), H \equiv H(|z_1|^2, |z_2|^2, |z_3|^2, |z_4|^2, \bar{z}_1 z_2 \bar{z}_3 z_4).$$

Here $H(\cdot)$ and $G(\cdot)$ are smooth complex-valued functions, and both functions are invariant under T_x, T_y, and T_t. To derive remaining components, z_i, $1 \leq i \leq 4$, we apply discrete reflection symmetries, R_x and R_y. For example,

$$g_2(z_1, z_2, z_3, z_4) = g_1(z_2, z_1, z_4, z_3).$$

Then the normal form (3.6) can be obtained by truncating $g_i(z_1, z_2, z_3, z_4)$, $1 \leq i \leq 4$, at the cubic order.

3.3.2 2D and 4D Invariant Subspaces

The system (3.6) is the normal form for a Hopf bifurcation with $\mathbb{O}(2)\times\mathbb{O}(2)$-symmetry posed in an eight-dimensional center eigenspace. In [49, 57] it is shown that to the action (3.7) there correspond (up to conjugacy) six distinct two-dimensional fixed points subspaces, which are invariant spaces for (3.6) and contain the basic periodic solutions whose existence is guaranteed by the equivariant Hopf bifurcation theorem [29]. These subspaces are summarized in Table 3.1(a). The differential equation for the complex variable z occurring in Table 3.1(a) is the normal form for a standard Hopf bifurcation,

$$\dot{z} = (a_0 + c|z|^2)z. \tag{3.8}$$

The periodic solutions of (3.8) have the form $z = re^{i\Omega T}$ with $r^2 = -a_{0r}/c_r$ and $\Omega = a_{0i} + c_i r^2$ (subscripts r and i denote real and imaginary parts). The names in Table 3.1(a) refer to the wave types associated with the periodic solutions residing in the fixed point subspaces via (2.4), and are related to the maximal isotropy subgroups of $\mathbb{O}(2) \times \mathbb{O}(2) \times \mathbb{S}^1$ fixing these patterns. Specifically, TW refers to oblique traveling waves fixed by spatiotemporal translations $T_{xt} : (x,t) \to (x + x_0, t - (p_c/\omega_c)x_0)$ and the corresponding translations T_{yt}; T_xR and T_yR refer to traveling rectangles in the x- and y-directions which are fixed by (T_{xt}, R_y) and (T_{yt}, R_x), respectively; SW refers to oblique standing waves fixed by $(x,y) \to (x + x_0, y - (p_c/q_c)x_0)$ and R_xR_y; SR refers to standing rectangles fixed by R_x and R_y; and AW refers to alternating waves characterized by periodic reversals between stripe patterns in the two oblique directions, which are fixed by R_x and R_y combined with a temporal phase shift by half the period.

In addition to the two-dimensional invariant subspaces, the system (3.6) has eight four-dimensional invariant subspaces fixed by non-maximal isotropy subgroups of $\mathbb{O}(2) \times \mathbb{O}(2) \times \mathbb{S}^1$. These subspaces are summarized in Table 3.1(b). When (3.6) is restricted to the first seven subspaces (S_{13} – S_{3+}) listed in this table, the system for the complex variables (z_1, z_2) becomes the normal form for a Hopf bifurcation with $\mathbb{O}(2)$-symmetry,

$$\begin{aligned} \dot{z}_1 &= (a_0 + A|z_1|^2 + B|z_2|^2)z_1, \\ \dot{z}_2 &= (a_0 + A|z_2|^2 + B|z_1|^2)z_2, \end{aligned} \tag{3.9}$$

with A, B summarized in the last column of the table. This system is known to have periodic solutions of the form $z_1 = re^{i\Omega T}$, $z_2 = 0$ and $z_1 = z_2 = re^{i\Omega T}$, which in the setting of 1D spatiotemporal systems correspond to traveling waves and standing waves, respectively. When (3.9) is defined by restricting (3.6), the traveling wave solutions are the basic periodic solutions listed first in the containment column of Table 3.1(b), and the standing wave solutions are the second. Generically these two

Table 3.1: (a) 2D invariant subspaces of (3.6) and coefficients c in (3.8). (b) 4D invariant subspaces of (3.6) and coefficients A, B in (3.9) and (3.10).

Name	Subspace	c
TW	$(z,0,0,0)$	a_1
T_yR	$(z,z,0,0)$	a_1+a_2
T_xR	$(z,0,0,z)$	a_1+a_4
SW	$(z,0,z,0)$	a_1+a_3
SR	(z,z,z,z)	$a_1+a_2+a_3+a_4+a_5$
AW	(z,iz,z,iz)	$a_1+a_2+a_3+a_4-a_5$

(a)

Name	Subspace	containments	A	B
S_{13}	$(z_1,z_2,0,0)$	TW, T_yR	a_1	a_2
S_{23}	$(z_1,0,z_2,0)$	TW, SW	a_1	a_3
S_{2-}	(z_1,iz_1,z_2,iz_2)	T_yR, AW	a_1+a_2	$a_3+a_4-a_5$
S_{3-}	(z_1,iz_2,z_2,iz_1)	T_xR, AW	a_1+a_4	$a_2+a_3-a_5$
S_{12}	$(z_1,0,0,z_2)$	TW, T_xR	a_1	a_4
S_{2+}	(z_1,z_1,z_2,z_2)	T_yR, SR	a_1+a_2	$a_3+a_4+a_5$
S_{3+}	(z_1,z_2,z_2,z_1)	T_xR, SR	a_1+a_4	$a_2+a_3+a_5$
S_1	(z_1,z_2,z_1,z_2)	SW, SR, AW	a_1+a_3	a_2+a_4

(b)

solutions are the only non-transient solutions of (3.9).

The only 4D invariant subspace that contains three basic periodic solutions is the subspace S_1 in Table 3.1(b). When restricted to S_1, (3.6) reduces to the normal form for a Hopf bifurcation with $\mathbb{D}_4$-symmetry,

$$\begin{aligned} \dot{z}_1 &= (a_0 + A|z_1|^2 + B|z_2|^2)z_1 + a_5\overline{z}_1 z_2^2, \\ \dot{z}_2 &= (a_0 + A|z_2|^2 + B|z_1|^2)z_2 + a_5\overline{z}_2 z_1^2, \end{aligned} \tag{3.10}$$

which describes a Hopf bifurcation with 4D center eigenspace in a system of four identical oscillators coupled with the symmetry of a square. At the Hopf bifurcation three different types of synchronization patterns are created, denoted rotating wave, vertex oscillation, and edge oscillation [29, 51], which in our case correspond to the SW, SR, and AW solutions, respectively. In addition to these basic solutions, which

reside in 2D invariant subspaces, an unstable periodic solution with lower symmetry and quasiperiodic solutions can exist in certain parameter regimes [51].

3.3.3 Complex Dynamics of the Normal Form

In a recent study [41] the coefficients a_j in (3.6) have been computed numerically from the governing partial differential equations of the WEM for a range of material parameters, and it was found that in a certain parameter regime none of the basic periodic solutions listed in Table 3.1(a) was stable. Instead, when one of the material parameters was varied, various quasiperiodic solutions and a period doubling cascade to chaotic dynamics did occur. In a subsequent parameter study of (3.6) [18], the coefficients a_0, a_{3i}, and a_1, a_2, a_4, a_5 have been fixed as

$$\begin{array}{lllllllll} a_0 & = & 1, & a_1 & = & -1-1.1806i, & a_4 & = & -0.2223-3.3025i, \\ a_{3i} & = & 1.3613, & a_2 & = & -0.923-0.5538i, & a_5 & = & -0.4647-0.2472i, \end{array} \tag{3.11}$$

and a_{3r} was varied in the range $0.1452 < -a_{3r} < 0.764$. In this range, which includes one of the values computed from the WEM, all six basic periodic solutions of (3.6) are unstable. At the left ($-a_{3r} = 0.1453$) and right ($-a_{3r} = 0.764$) ends the SW and T_xR solutions become stable, respectively. When $-a_{3r}$ is increased above 0.1453, periodic solutions not residing in any fixed point subspace and various quasiperiodic solutions occur as attractors for $-a_{3r} < 0.6374$. Note that, due to the S^1-action, periodic solutions of (3.6) are actually relative equilibria, and the quasiperiodic solutions found in [41, 18] are relative periodic orbits [11]. In particular, in this range a relative periodic orbit in S_1 occurs, which becomes transversely unstable and leads to a stable relative periodic orbit outside of S_1.

In the range $0.6374 < -a_{3r} < 0.764$, the dynamics of (3.6) is complex. The characteristics of this dynamics are chaos, intermittency, and periodic windows terminating or starting in period doubling cascades, and both periodic and chaotic attractors occur

in symmetric and asymmetric (as defined below) forms. To visualize the dynamics, symmetry adapted, 'projective' variables have been introduced in [18] as follows,

$$D_j = d_j/s,\ 1 \le j \le 3, \quad U = u/s^2,\ \ V = v/s^2, \tag{3.12}$$

where $z_j = r_j e^{i\varphi_j}$,

$$\begin{aligned} d_1 &= r_1^2 - r_2^2 + r_3^2 - r_4^2, & u &= \mathrm{Re}(\overline{z_1 z_3} z_2 z_4) = r_1 r_2 r_3 r_4 \cos\phi, \\ d_2 &= r_1^2 + r_2^2 - r_3^2 - r_4^2, & v &= \mathrm{Im}(\overline{z_1 z_3} z_2 z_4) = r_1 r_2 r_3 r_4 \sin\phi, \\ d_3 &= r_1^2 - r_2^2 - r_3^2 + r_4^2, & s &= r_1^2 + r_2^2 + r_3^2 + r_4^2. \end{aligned} \tag{3.13}$$

and

$$\varphi = -\varphi_1 + \varphi_2 - \varphi_3 + \varphi_4, \tag{3.14}$$

which leads to a closed system of differential equations for (d_j, u, v, s). In the resulting system for (D_j, U, V), the variable s appears as an overall factor which can be formally removed by a time rescaling leading to a reduction of the phase-space dimension to five. Moreover, these variables satisfy the relation $256(U^2+V^2) = (r_1 r_2 r_3 r_4)^2/s^2 \equiv P$ with P depending on the D_j only, which reduces the dimension to four. If all moduli r_j are nonzero, one can set $(U, V) = \sqrt{P}(\cos\varphi, \sin\varphi)$ and visualize the dynamics in (D_j, φ)-space.

The continuous symmetries T_x, T_y, S^1 all act trivially on the reduced variables (d_j, u, v, s) or (D_j, U, V) corresponding to an orbit space reduction [11], whereas the discrete symmetries act as (we set $R_{xy} = R_x R_y$),

$$\begin{aligned} R_x(d_1, d_2, d_3, v) &= (-d_1, d_2, -d_3, -v), \\ R_{xy}(d_1, d_2, d_3, v) &= (d_1, -d_2, -d_3, v), \\ R_y(d_1, d_2, d_3, v) &= (-d_1, -d_2, d_3, -v), \end{aligned} \tag{3.15}$$

and leave s and u invariant (the actions on (D_j, U, V) are identical). Thus the reduced systems for (d_j, u, v, s) or (D_j, U, V) retain a $\mathbb{D}_2$-equivariance. In these variables, relative equilibria are revealed as equilibria and relative periodic orbits as periodic orbits.

In [18] it has been observed that in the complex regime chaotic and periodic attractors occur in pairs distinguished by $d_3 > 0$ and $d_3 < 0$. If $\mathcal{A}$ is an attractor in $d_3 > 0$, say, $R_x\mathcal{A}$ and $R_{xy}\mathcal{A}$ are conjugate attractors in $d_3 < 0$. An attractor in $d_3 > 0$ was called symmetric in [18] if $R_y\mathcal{A} = \mathcal{A}$ and asymmetric if $R_y\mathcal{A} \cap \mathcal{A} = \emptyset$. Thus in the complex regime, the normal form in the reduced phase space exhibits either two symmetric (with respect to R_y) attractors or four asymmetric attractors (multi-stability of non-conjugate attractors has not been observed in the complex regime). Bifurcations in which a pair of asymmetric chaotic attractors merge in a single symmetric chaotic attractor are called symmetry increasing bifurcations, and a bifurcation in which a symmetric periodic orbit becomes unstable and two stable asymmetric periodic orbits are created is called a symmetry breaking bifurcation [28]. Note that, if $P = (d_j, u, v, s)$, a symmetric periodic orbit $X(T)$ with minimal period T_p satisfies $R_y P(T + T_p/2) = P(T)$.

The periodic orbit bifurcating out of S_1 is symmetric, and undergoes a symmetry breaking bifurcation at $-a_{3r} = 0.6374$. When $-a_{3r}$ is increased above this value, the first period doubling cascade starts at $-a_{3r} \approx 0.64308$ and accumulates at $-a_{3r} \approx 0.64418$. The resulting asymmetric chaotic orbit for $-a_{3r} = 0.6442$ is displayed in Figure 3.4.

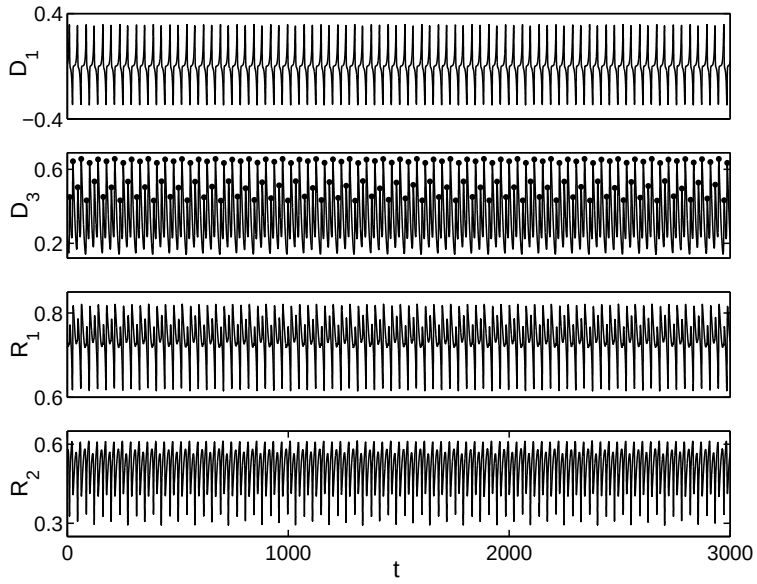

(a)

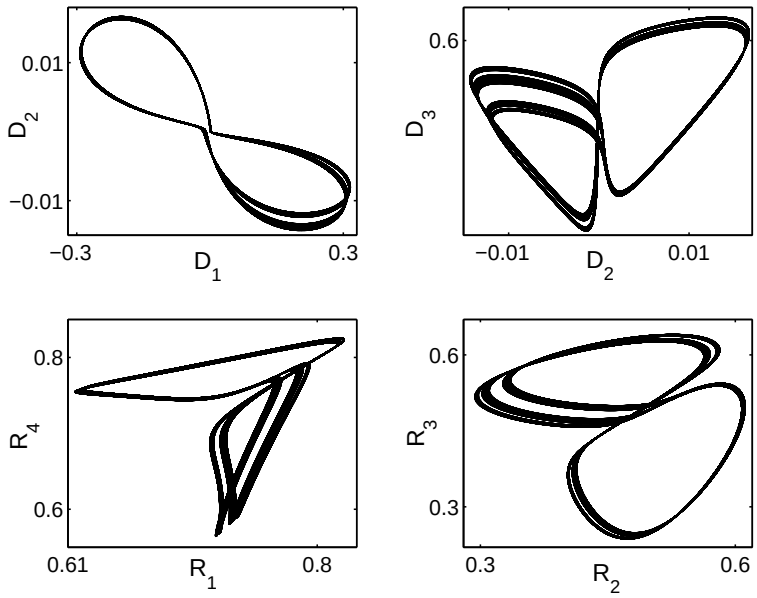

(b)

Figure 3.4: Asymmetric chaotic attractor of the unperturbed normal form (3.6) for $-a_{3r} = 0.6442$. (a) Time series ($R_j = |z_j|$), (b) Phase plane plots. The dots in $D_3(T)$ mark local maxima, which have been used in [18] to define a Poincaré map.

3.4 Intermitency

3.4.1 Introduction to Intermittency: Pomeau-Manneville Intermittency

Time plots of the first order X-modes in Figure 3.3 illustrate intermittent behavior: phases of periodic or nearly periodic dynamics are randomly interrupted by sudden bursts. The word intermittency was used in fluid dynamics to describe signals from probes alternating between flat portions and burst ones, which are defined as laminar phases and turbulent phases. Pomeau and Manneville are pioneers for modeling and analysis of intermittent behavior. In [37, 45] they studied intermittency in the Lorenz system

$$\begin{aligned} \dot{x} &= \sigma(y - z), \\ \dot{y} &= -xz + rx - y, \\ \dot{z} &= xy - bz, \end{aligned}$$

by taking $\sigma = 10$, $b = 8/3$, and varying r from 166 to 167. Figure 3.5 shows a transition from a limit cycle to a strange attractor at $r = 166.07$ for the time series of z. Turbulent bursts randomly interrupt the stable limit cycle for $r < 166.07$. The durations of the laminar phases are shorter and shorter as r is increased. Pomeau and Manneville applied several Poincaré maps to investigate this so-called intermittency phenomenon. By choosing the plane $x = 0$ as the surface of section, the transformation $(y_{n+1}, z_{n+1}) = f(y_n, z_n)$ is obtained by connecting a given intersection of the trajectory with the Poincaré section with the next one in the course of the motion. Moreover, a simpler picture in terms of the transformation $y_{n+1} = f(y_n)$ can be derived from the transformation $(y_{n+1}, z_{n+1}) = f(y_n, z_n)$ by choosing another Poincaré section in which z_n is constant. The resulting roughly smooth single valued function

of y_n, which is provided in Figure 3.6, is nearly tangent to $y_{n+1} = y_n$. We transform solutions from differential equations to data from iterative maps, then we can apply the knowledge from dynamics of maps to investigate the above transition.

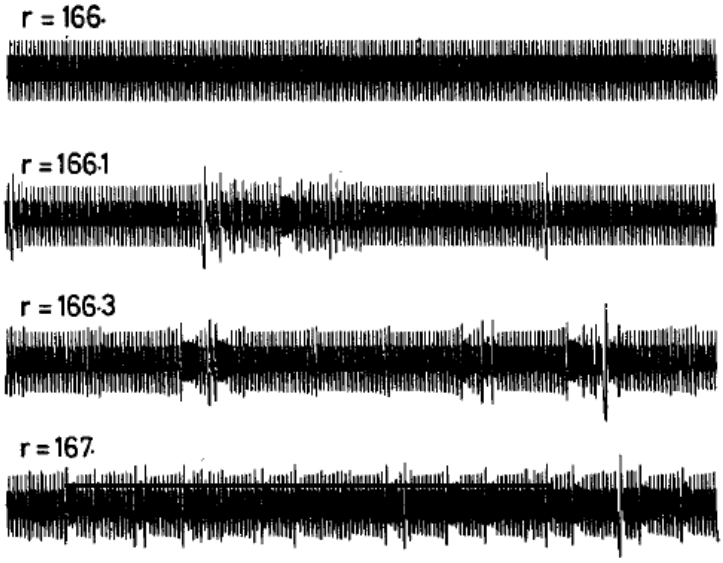

Figure 3.5: Time series of z in the Lorenz model, from [37].

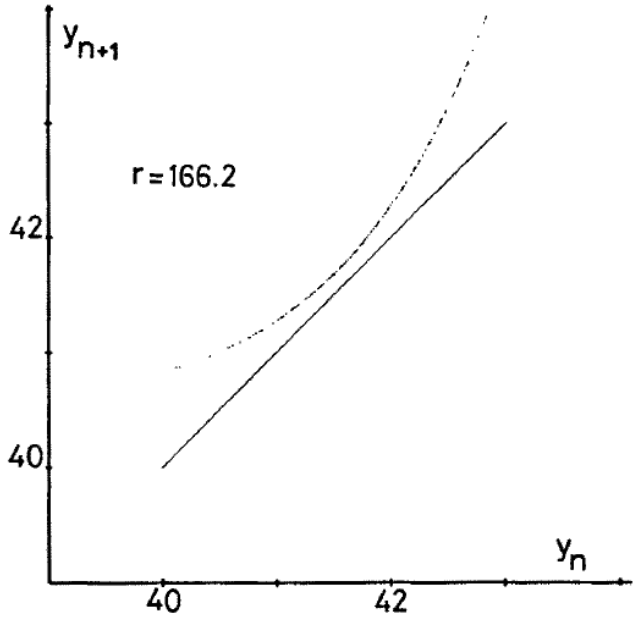

Figure 3.6: A part of the Poincaré map along the y-coordinate for $r = 166.2$ slightly beyond the intermittency threshold ($r_T \approx 166.06$), from [45].

The idealized picture of $y_{n+1}(y_n)$ explaining the transition via intermittency is presented in Figure 3.7 [45]. For r slightly below r_T, which is the critical value for the tangent bifurcation, this curve has two intersections with the identity map $y_{n+1} = y_n$, corresponding to stable and unstable limit cycles in the continuous system from which the map is derived. They collapse into a single point at $r = r_T$ via saddle-node bifurcation, which is also called tangent bifurcation. For $r > r_T$, the curve is lifted up and no longer crosses the identity map so that a channel appears between them. The trajectory drifts slowly upwards through the channel. The time taken to pass through it depends on the channel width. So that the narrower the channel is, the longer the laminar time lasts. A generic form

$$y_{n+1} = y_n + y_n^2 + \epsilon + \text{h.o.t}$$

can be used to estimate the time, where $\epsilon = (r - r_T)/r_T$. It is estimated that the number of iterations needed to cross the channel is of the order $\sqrt{\epsilon}$ by approximating the difference equation by a differential equation. Therefore, the average time between bursts is proportional to $\epsilon^{-1/2}$. Moreover, the probability that a laminar phase has exactly length n has a power law with exponent $-1/2$, and the Lyapunov number varies as $\sqrt{\epsilon}$.

The above intermittency is called Type I Pomeau-Manneville intermittency, where a real Floquet multiplier crosses the unit circle at $+1$, i.e. tangent bifurcation. The reinjection mechanism is another ingredient, reintroducing the trajectory to the vicinity of the channel once it has escaped. Otherwise the iterates diverge from the channel and never revisit the neighborhood of interest. Authors in [45] also investigated Type II intermittency, occurring when a Floquet multiplier passes through the unit circle as a complex conjugate pair, which is called a Hopf bifurcation, and Type III intermittency, taking place when a real Floquet multiplier crosses the unit circle at -1,

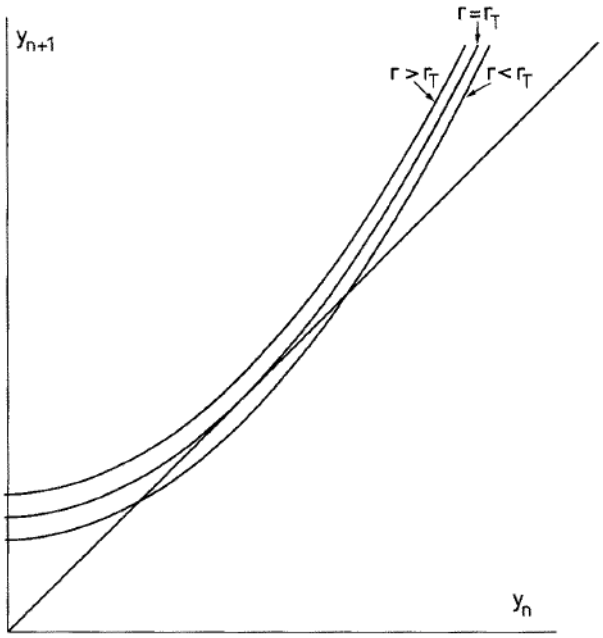

Figure 3.7: Idealized picture of $y_{n+1}(y_n)$ explaining the transition via intermittency, from [45].

i.e., inverse period doubling bifurcation. Extensions of Type I intermittency include Type X intermittency [46] and Type V intermittency [7]. For Type X intermittency, the reinjection point is close to the unstable point resulting from a saddle node bifurcation. Therefore, the laminar time is not controlled by the channel width, like Type I intermittency, but by the proximity of the reinjection point to the unstable fixed point, and by the gradient of the return map in that region. The name of this intermittency type is from the X-shaped iterative map. Type V intermittency is generated by destroying the stability of the fixed point from a saddle node bifurcation by colliding with a point of discontinuity. Statistical features, such as dependence of the average laminar length on the control parameter, and scaling power-law, are provided in [46, 7].

3.4.2 Intermittency from the Invariant Manifold: In-Out Intermittency

Previous pioneering work in intermittency has been done for fixed values of the local bifurcation parameter. However, in Figure 3.3 the noncentral modes in the Ginzburg Landau system (2.11) display intermittency relative to an invariant manifold (the normal form). Here we discuss intermittency involving an invariant manifold in detail.

Suppose there is an invariant manifold and a corresponding attractor when the dynamics is restricted to it. The transverse stability of such an attractor can be determined by the largest normal Lyapunov exponent for the natural measure on this attractor [4]. If the largest normal Lyapunov exponent is negative, the attractor is transversely stable. If the largest normal Lyapunov exponent is positive, the attractor in the invariant manifold is a chaotic saddle in the full space, and intermittency appears.

There are two types of intermittency involving invariant manifolds: on-off intermittency [30, 44, 56] and in-out intermittency [5, 12]. The author in [3] distinguished them in Figure 3.8 as following: let A be the attractor in the full space, M_I be the invariant subspace, and $A_0 = A \cap M_I$. And let A_0^* be the attractor in M_I for the dynamics restricted to the invariant subspace M_I. If $A_0^* = A_0$, we say the attractor A displays on-off intermittency. If $A_0^* \subset A_0$ then we say that A displays in-out intermittency. It is proved in [5] that in-out intermittency cannot occur in a skew product system. As pointed out in [3], the skew product means dynamics within the invariant manifold is independent of dynamics in the transverse direction, which has nothing to do with skew symmetric matrices.

A schematic representation of the mechanism generating in-out intermittency is depicted in Figure 3.9 from [12]. The attractors in the invariant subspace are not necessarily chaotic. They are often periodic or equilibria. The trajectory remains close to one of these attractors during the out phases, with the important consequence

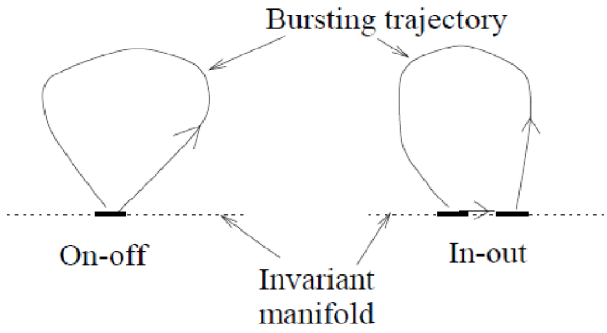

Figure 3.8: Schematic difference between on-off intermittency and in-out intermittency, from [3]. There is only one invariant set attracting and repelling transversely for on-off intermittency. For in-out intermittency there is more than one invariant set in the invariant manifold with attraction and repulsion relative to the invariant manifold.

that during these out phases the trajectory can shadow a periodic orbit, while drifting away from the invariant subspace at an exponential rate. For parameters chosen in (3.4) for Ginzburg Landau equations, Figure 3.2 and Figure 3.4 demonstrate that within the invariant manifold (the normal form), there are two symmetry-related chaotic sets, which are transversely unstable, and one invariant set, origin, which is transversely stable. Therefore intermittency in Ginzburg Landau equations is of in-out type.

In order to reduce the number of variables in the expansion of the spatiotemporal chaotic pattern (3.1) and characterize the switching dynamics inside the invariant manifold and the bursting dynamics outside the invariant manifold, we just focus on the central modes and the modes in X-direction, since all noncentral modes in Y-direction vanish. Motivated by Figure 3.2 and normal form symmetry-adapted variables (3.13), we introduce the following symmetry-adapted variables for the modes in the expansion (3.1),

$$\begin{aligned} d_0 &= |a^{(1)}_{(0,0)}|^2 - |a^{(2)}_{(0,0)}|^2 - |a^{(3)}_{(0,0)}|^2 + |a^{(4)}_{(0,0)}|^2, \\ d_1 &= |a^{(1)}_{(1,0)}|^2 - |a^{(2)}_{(1,0)}|^2 - |a^{(3)}_{(1,0)}|^2 + |a^{(4)}_{(1,0)}|^2, \end{aligned} \tag{3.16}$$

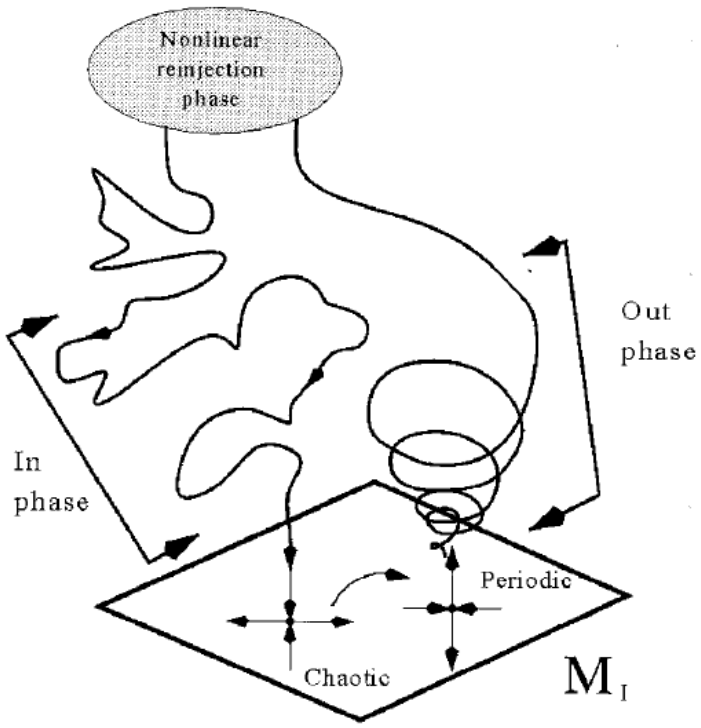

Figure 3.9: A schematic representation of in-out intermittency, from [12].

where d_1 is representative for all noncentral modes regarding the x-reflection symmetry, because all noncentral modes in X-direction behave qualitatively similarly and decay very quickly with increasing order, and d_0 characterizes dynamics of the normal form variables regarding the x-reflection symmetry. Notice that d_1 describes the bursting dynamics in the transverse direction of the invariant manifold, and $d_1 = 0$ is the invariant manifold where the switching dynamics of the central modes occurs. Based on (3.16), we see that switches occur between the negative and positive symmetry-related components of d_0, and $\mathbb{O}(2) \times \mathbb{O}(2)$-symmetry in (2.11) is reduced to $\mathbb{Z}(2)$ symmetry:

$$(d_0, d_1) \quad \rightarrow \quad (-d_0, -d_1). \tag{3.17}$$

Our goal here is to provide a low dimensional map to characterize the bursting-switching dynamics in the Ginzburg Landau system. We need to simplify the dynam-

ics concerning d_0 and d_1 from the continuous differential equations to discrete data by the following Poincaré map:

$$\dot{d}_0 = 0, \quad \ddot{d}_0 d_0 < 0, \tag{3.18}$$

which corresponds to local maximum values of d_0, if $d_0 > 0$ and local minimum values of d_0, if $d_0 < 0$. Time series and the phase portrait from the Poincaré map (3.18) are provided in Figure 3.10. Time series of the Poincaré map (Figure 3.10(a)) indicates that when the dynamics is restricted to the invariant manifold, there exist two symmetry-related chaotic sets and an unstable equilibrium 0. These two chaotic invariant sets are unstable in the transverse direction. Therefore the transverse variable d_1 can get active and escape from the invariant manifold. On the other hand, even though $d_0 = 0$ is unstable within the invariant manifold, it is attractive in the transverse direction. Therefore, d_1 is attracted back to the invariant manifold at $d_0 = 0$, and then the trajectory moves to the chaotic sets. These two chaotic sets and $d_0 = 0$ form a heteroclinic orbit in the full space. The symmetry (3.17) forces the trajectory starting on the positive chaotic set to move to positive d_1, and the one starting on the negative chaotic set to move to negative d_1. This is in-out intermittency, since the intersection of the attractor of the full system and invariant manifold, A_0, is not a minimal attractor, i.e., $d_0 = 0$ is not an attractor on A_0. Figure 3.10(b) shows that the normal form $d_1 = 0$ is an invariant manifold.

The bursting-switching dynamics in the Poincaré map (3.18) from the Ginzburg Landau system can be modeled by the following two-dimensional map:

$$\begin{aligned} X &\to [r\exp(-aY^2) + s(1-\exp(-aY^2))]X - X^3, \\ Y &\to \tfrac{\arctan(\theta X)}{\pi/2}[(\mu - \gamma\exp(-bX^2))|Y| - Y^2], \end{aligned} \tag{3.19}$$

where

$$\begin{aligned} a &= 100, \quad b = 10, \quad r = 3\sqrt{3}/2 - 0.1, \quad s = -0.5, \\ \theta &= 100, \quad \mu = 1.5, \quad \gamma = 1. \end{aligned} \tag{3.20}$$

The map (3.19) uses X to produce the dynamics of d_0, Y to mimic d_1, and $Y = 0$ forms an invariant manifold, on which X follows a cubic logistic (unimodal) map,

$$X \to rX - X^3.$$

This construction is motivated by Figure 3.11 when the dynamics is restricted to the invariant manifold: when r is given as the value in (3.20), two symmetry-related chaotic sets, i.e. $X \to -X$, appear based on corresponding initial conditions, while $X = 0$ is an unstable equilibrium point of the cubic map. We denote the positive chaotic set by C_+ and the negative one by C_-. When the transverse variable Y gets active, the growth of Y induce switchings of X-variable between the positive and negative chaotic sets, once

$$[r\exp(-aY^2) + s(1 - \exp(-aY^2))] < X^2.$$

For the transverse variable Y, we construct it to be transversely unstable on both chaotic sets $C_\pm$, and transversely stable at the equilibrium point $X = 0$. The choice of $(\mu - \gamma\exp(-bX^2))$ in (3.19) realizes the above consideration by taking appropriate b-value, such that on $C_\pm$ the linear part is μ, which is bigger than 1, while on $X = 0$ the linear coefficient is $\mu - \gamma$, which is smaller than 1. The nonlinear term $-Y^2$ serves as a reinjection mechanism. The absolute value of Y component and $\frac{\arctan(\theta X)}{\pi/2}$ are constructed from symmetry considerations. Notice that $\frac{\arctan(\theta X)}{\pi/2} \approx 1$ on C_+ and ≈ -1 on C_-. Time series and phase portrait for (3.19) with parameters given in (3.20) are presented in Figure 3.12(a) and (b).

The low dimensional map (3.19) captures the dynamics within the invariant manifold $Y = 0$ as a unimodal chaotic map, leading to two chaotic sets unstable in the transverse direction. The resulting bursts from the invariant manifold "break" these two chaotic sets, and induce switches. In order to investigate how the noncentral modes affect the dynamics of the central modes and induce switches between a pair of symmetry-conjugated chaotic saddles in the invariant manifold formed by the four central modes for the Ginzburg Landau system (2.11), we study a low dimensional model, which is an extension of the normal form with one translation symmetry breaking terms included, in the following Chapter.

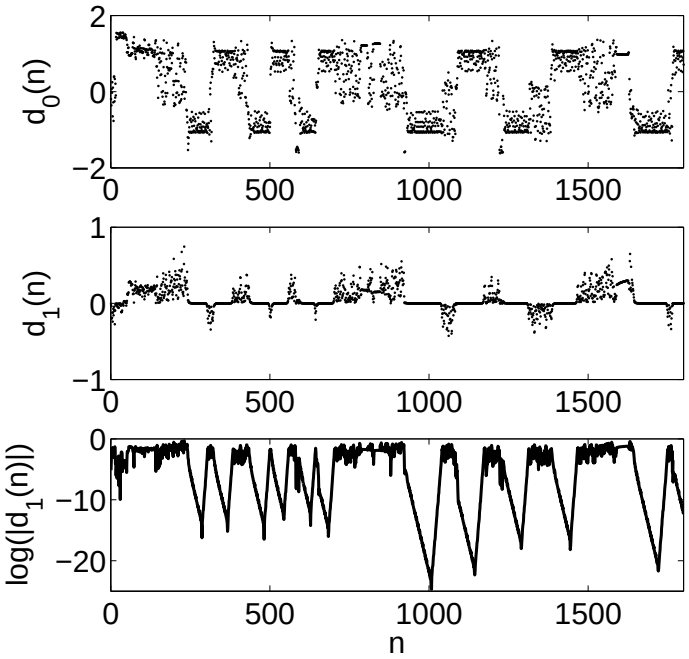

(a)

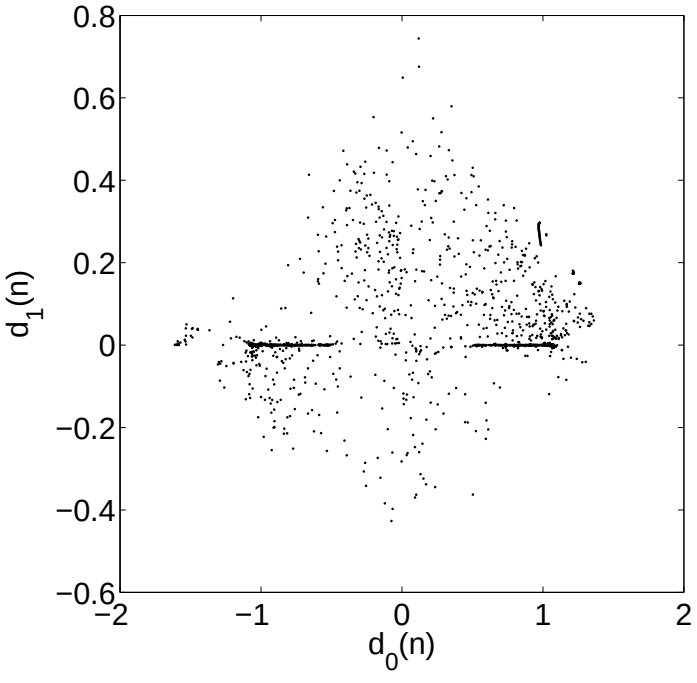

(b)

Figure 3.10: Data of Poincaré map (3.18) regarding symmetry-adapted variables (3.16). (a): Time plots of Poincaré map of d_0 and d_1, the exponential rate of "out" and "in" phases indicate this is in-out scenario. (b): Phase plane plots of Poincare map of d_0 and d_1.

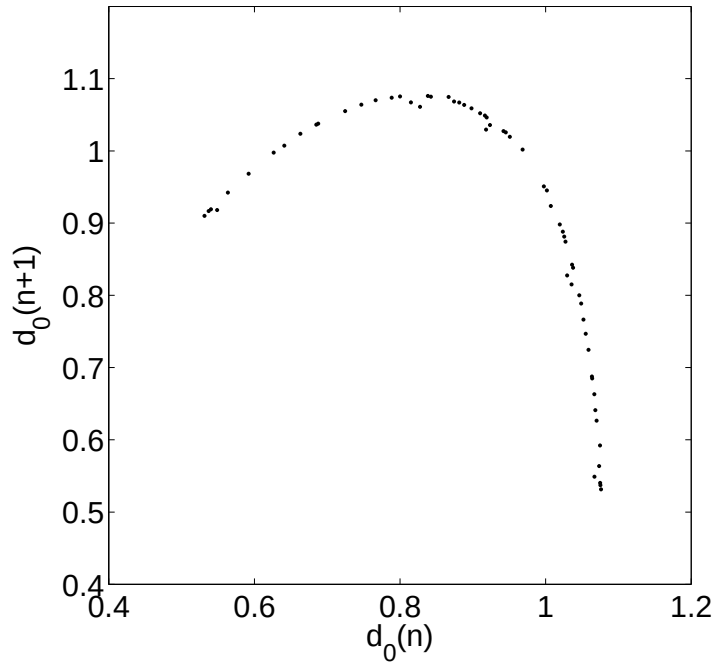

(a)

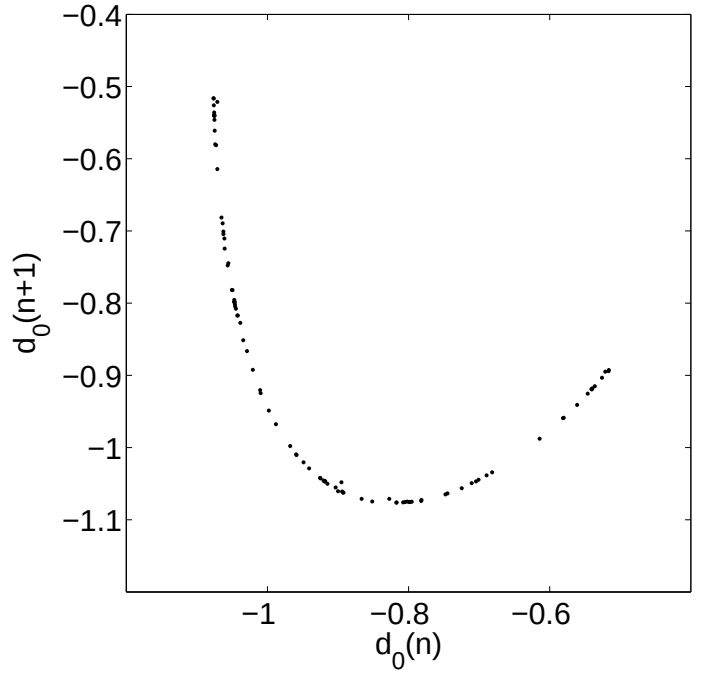

(b)

Figure 3.11: Iterates of the Poincaré map of $d_0(n+1)$ versus $d_0(n)$ for positive (a) and negative (b) d_0, respectively, while dynamics is restricted in the invariant manifold $d_1 = 0$.

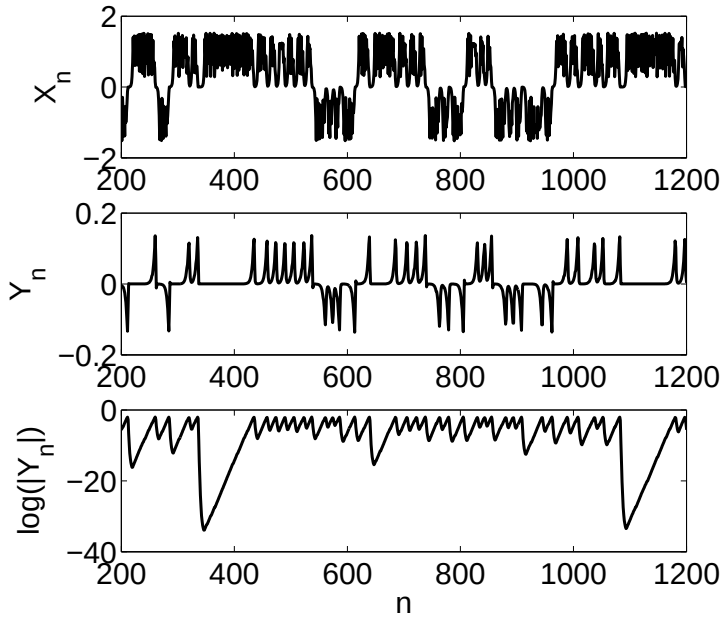

(a)

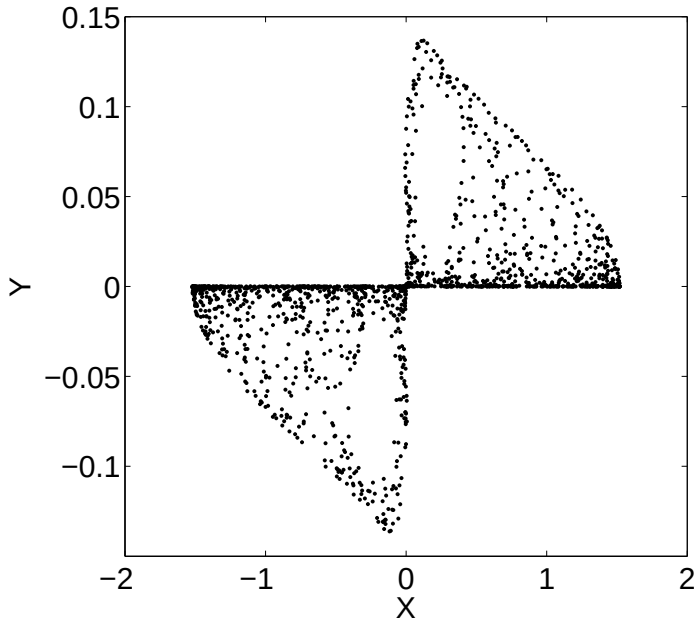

(b)

Figure 3.12: Time series and phase portrait for (3.19) with parameters given in (3.20). (a) Time series of X and Y for (3.19), the log scale of Y indicates this is in-out type. (b) Phase plane plots of X versus Y.

Chapter 4

Perturbed Normal Form

4.1 Introduction

In Chapter 3 we identify an invariant manifold in the STC and reveal that the STC is due to in-out intermittency caused by transverse instability of the invariant manifold. The bursts of the transverse variables induce switchings between a pair of symmetry-conjugated chaotic saddles in the invariant manifold (see Figure 3.2). In this chapter we present a low dimensional model, a normal form for a Hopf bifurcation with a broken translation invariance posed in the space of the central modes, to understand the instability mechanism causing the switching dynamics found in the Ginzburg Landau system.

The model, inferred from the form of the equations for the mode amplitudes $a^{(j)}_{m,n}$ (3.2), preserves the reflection symmetries and the Hopf normal form symmetry. Since the Y-modes decay to zero, we include only the $a^{(j)}_{m,0}$ and for simplicity only the first harmonics, $m = 0, \pm 1$. We set $z_j = a^{(j)}_{0,0}$ and $\xi_{j\pm} = a^{(j)}_{\pm 1,0}$ and treat the $\xi_{j\pm}$ as small constants. If both ξ_{j+} and ξ_{j-} are nonzero, the equation for z_1 contains the terms $2a_1\xi_{1+}\xi_{1-}\overline{z}_1 + a_4(\xi_{1+}\xi_{4-} + \xi_{4+}\xi_{1-})\overline{z}_4$ that break the $\mathbb{S}^1$-symmetry, thus one of ξ_{j+} or ξ_{j-} must be zero. Denoting by ξ_j the nonzero first harmonic, in order that the

reflection symmetries are preserved the ξ_j must be identical for all j. Thus, setting $\xi_j = b$, the perturbation terms in the z_1-equation reduce to $\beta z_1 + (a_4 + a_5)|b|^2 z_4$, where $\beta = (2a_1 + a_2 + a_3 + a_4)|b|^2$. Since β can be absorbed into a_0, our perturbed normal form takes the form,

$$\begin{aligned}
\dot{z}_1 &= a_0 z_1 + \theta z_4 + (a_1|z_1|^2 + a_2|z_2|^2 + a_3|z_3|^2 + a_4|z_4|^2)z_1 + a_5 z_2 \overline{z}_3 z_4, \\
\dot{z}_2 &= a_0 z_2 + \theta z_3 + (a_1|z_2|^2 + a_2|z_1|^2 + a_3|z_4|^2 + a_4|z_3|^2)z_2 + a_5 z_1 \overline{z}_4 z_3, \\
\dot{z}_3 &= a_0 z_3 + \theta z_2 + (a_1|z_3|^2 + a_2|z_4|^2 + a_3|z_1|^2 + a_4|z_2|^2)z_3 + a_5 z_4 \overline{z}_1 z_2, \\
\dot{z}_4 &= a_0 z_4 + \theta z_1 + (a_1|z_4|^2 + a_2|z_3|^2 + a_3|z_2|^2 + a_4|z_1|^2)z_4 + a_5 z_3 \overline{z}_2 z_1,
\end{aligned} \tag{4.1}$$

where $\theta = (a_4 + a_5)|b|^2$. The results of simulations of (4.1) for $b = 0.2$ are shown in Figure 4.1. We observe here similar switching dynamics as in our simulations of the Ginzburg Landau system (Figure 3.2), confirming that (4.1) provides a low-dimensional model for this kind of dynamics. We analyze this similarity in what follows.

For arbitrary complex θ, the perturbation terms in (4.1) are generic linear terms that break the y-translation invariance T_y. Thus the perturbed normal form can also be considered as an imperfect version of the normal form for a Hopf bifurcation with one broken translation (or circular) symmetry. Investigating the effect of breaking a translation symmetry in (3.6) is another motivation for studying (4.1), which is related to a similar study pursued in [20], where the effect of breaking a translation symmetry on the Hopf bifurcation with $\mathbb{O}(2)$-symmetry has been investigated. The study of [20] was motivated by setting up a low-dimensional model describing the effect of distant sidewalls, which obviously breaks the translation invariance, on an oscillatory instability in a 1D extended spatial system. One of the results of this study was the identification of a solution that remarkably well resembles the so called blinking state observed in convection experiments in binary fluids.

In our case the symmetry breaking terms can be considered as the effect of distant

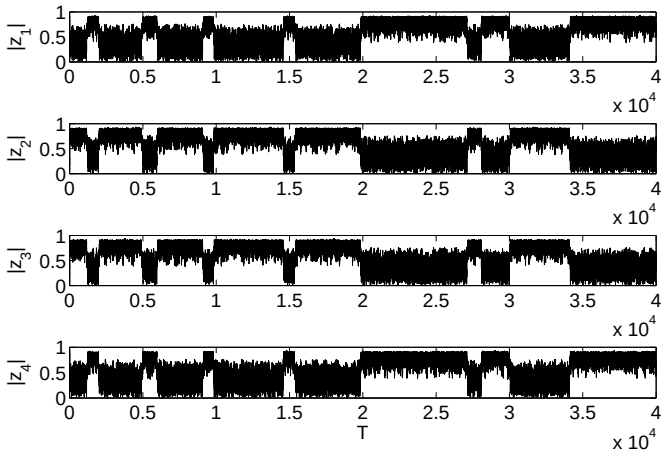

(a)

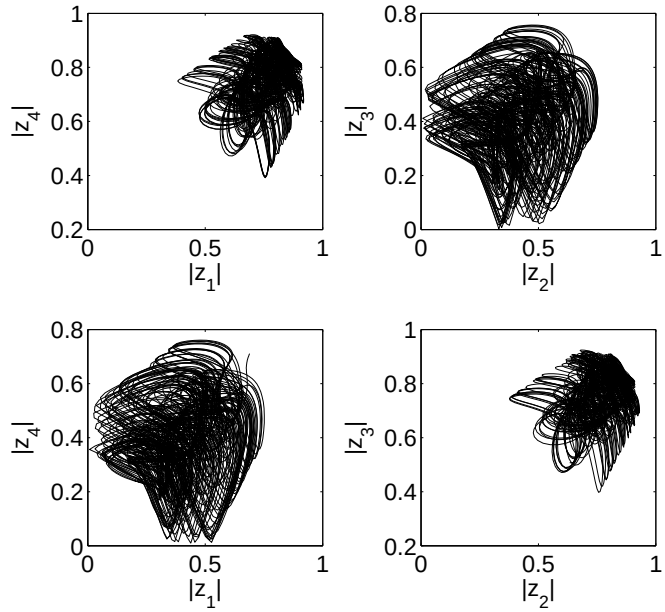

(b)

Figure 4.1: (a) Time series computed from the perturbed normal form (4.1) for a_j as used in (3.6) and (2.11) for Figures 3.4 and 3.2, with $b = 0.2$. (b) Phase plane portraits corresponding to (a) for the time ranges $20,000 \leq T \leq 22,000$ (upper panels) and $10,000 \leq T \leq 12,000$ (lower panels).

sidewalls in the y-direction on an oscillatory instability in a 2D extended anisotropic system [40]. Breaking only one translation invariance means the system has a large aspect ratio. Another setting that leads to (4.1) is a system posed in a large but finite cylinder [31]. Here the $\mathbb{O}(2)$-symmetry in the x-direction is a true geometrical symmetry, whereas the broken $\mathbb{O}(2)$-symmetry in the y-direction results from finite size effects captured by including symmetry breaking terms as in [20].

4.2 Symmetry Adapted Real Variables

The system (4.1) is difficult to analyze due to its high dimensionality. Polar coordinates, $z_j = r_j \exp(i\varphi_j)$, $1 \leq j \leq 4$, can be applied to reduce the original eight dimensional system to the following one,

$$\begin{aligned}
\dot{r}_1 &= (a_{0r} + a_{1r}r_1^2 + a_{2r}r_2^2 + a_{3r}r_3^2 + a_{4r}r_4^2)r_1 + r_2r_3r_4(a_{5r}\cos(\varphi) + a_{5i}\sin(\varphi)) \\
&\quad + r_4(\theta_r\cos(\varphi_1 - \varphi_4) + \theta_i\sin(\varphi_1 - \varphi_4)), \\
\dot{\varphi}_1 &= a_{0i} + a_{1i}r_1^2 + a_{2i}r_2^2 + a_{3i}r_3^2 + a_{4i}r_4^2 + \tfrac{r_2r_3r_4}{r_1}(a_{5i}\cos(\varphi) + a_{5r}\sin(\varphi)) \\
&\quad + \tfrac{r_4}{r_1}(\theta_i\cos(\varphi_4 - \varphi_1) + \theta_r\sin(\varphi_4 - \varphi_1)),
\end{aligned} \tag{4.2}$$

where $\varphi = -\varphi_1 + \varphi_2 - \varphi_3 + \varphi_4$. Equations for r_j and φ_j, where $2 \leq j \leq 4$, can be derived from symmetry considerations. Notice that just two phase variables, $\zeta = \varphi_1 - \varphi_4$, $\eta = \varphi_3 - \varphi_2$, are needed in the system (4.2). To avoid singularity and reduce the dimension further, the symmetry-adapted variables d_1, d_2, d_3 from (3.13) are used. Instead of u and v in (3.13), we use two pairs of phase-related variables u_k, v_k, $k = 1, 2$, defined by

$$\begin{aligned}
u_1 &= r_1r_4\cos(\zeta) - r_2r_3\cos(\eta), \quad v_1 = r_1r_4\sin(\zeta) - r_2r_3\sin(\eta), \\
u_2 &= r_1r_4\cos(\zeta) + r_2r_3\cos(\eta), \quad v_2 = r_1r_4\sin(\zeta) + r_2r_3\sin(\eta),
\end{aligned} \tag{4.3}$$

The system of equations (4.1) becomes,

$$\begin{aligned}
\dot{d}_1 &= 2a_{0r}d_1 + b_{01}sd_1 + b_{23}d_2d_3 - 4a_{5i}(u_1v_1 - u_2v_2) + 4\theta_i v_2,\\
\dot{d}_2 &= 2a_{0r}d_2 + b_{02}sd_2 + b_{13}d_1d_3 + 4\theta_i v_1,\\
\dot{d}_3 &= 2a_{0r}d_3 + b_{03}sd_3 + b_{12}d_1d_2 + 4\theta_r u_1,\\
\dot{s} &= 2a_{0r}s + (b_0s^2 + b_1d_1^2 + b_2d_2^2 + b_3d_3^2)/2 + 2a_{5r}(v_1^2 + u_2^2 - u_1^2 - v_2^2) + 4\theta_r u_2,\\
\dot{u}_1 &= 2a_{0r}u_1 + \alpha_1 su_1 - \beta_1 d_1v_1 + \delta_2 d_3u_2 - \gamma_2 d_2v_2 + \theta_r d_3,\\
\dot{v}_1 &= 2a_{0r}v_1 + \alpha_2 sv_1 + \beta_2 d_1u_1 + \delta_1 d_3v_2 + \gamma_1 d_2u_2 - \theta_i d_2,\\
\dot{u}_2 &= 2a_{0r}u_2 + \alpha_2 su_2 - \beta_2 d_1v_2 + \delta_1 d_3u_1 - \gamma_1 d_2v_1 + \theta_r s,\\
\dot{v}_2 &= 2a_{0r}v_2 + \alpha_1 sv_2 + \beta_1 d_1u_2 + \delta_2 d_3v_1 + \gamma_2 d_2u_1 - \theta_i d_1,
\end{aligned} \tag{4.4}$$

where

$$\begin{aligned}
&c_0 = a_1 + a_2 + a_3 + a_4, && c_1 = a_1 - a_2 + a_3 - a_4,\\
&c_2 = a_1 + a_2 - a_3 - a_4, && c_3 = a_1 - a_2 - a_3 + a_4,\\
&c_{kl} = (c_k + c_l)/2, \ \ 0 \le k,\ l \le 3
\end{aligned} \tag{4.5}$$

b_k and b_{kl} are real parts of c_k and $c_{k,l}$, i.e., $b_k = c_{kr}$ and $b_{kl} = c_{klr}$, and

$$\begin{aligned}
\alpha_k &= (c_{0r} + (-1)^k a_{5r})/2, \quad \beta_k = (c_{1i} + (-1)^k a_{5i})/2,\\
\delta_k &= (c_{3r} + (-1)^k a_{5r})/2, \quad \gamma_k = (c_{2i} + (-1)^k a_{5i})/2,
\end{aligned}$$

for $k = 1, 2$. The variables u_1, u_2, v_1, and v_2 are not independent, but satisfy two relations

$$\begin{aligned}
(u_1 + u_2)^2 + (v_1 + v_2)^2 &= 4r_1^2r_4^2 = (s + d_1 + d_2 + d_3)(s - d_1 - d_2 + d_3)/4,\\
(u_1 - u_2)^2 + (v_1 - v_2)^2 &= 4r_2^2r_3^2 = (s + d_1 - d_2 - d_3)(s - d_1 + d_2 - d_3)/4.
\end{aligned}$$

Therefore we reduce the eight dimensional system (4.1) to the six dimensional one (4.4).

Symmetry-adapted variables in (4.3) are invariant under T_x and S^1 in (3.7).

Symmetry-breaking terms split the phase variable, $\varphi = -\varphi_1 + \varphi_2 - \varphi_3 + \varphi_4$, into two parts, $\zeta = \varphi_1 - \varphi_4$ and $\eta = \varphi_3 - \varphi_2$, and symmetry-adapted variables associated with phases ζ and η, u_1, u_2, v_1, and v_2, are not invariant under T_y anymore, compared with the action of T_y in the normal form, because y-translation symmetry is not present in (4.4) anymore. Reflection actions, R_x, R_y, and R_{xy}, in (3.7), keep s and u_2 invariant, while other variables are transformed as

$$\begin{aligned} R_x(d_1, d_2, d_3, u_1, v_1, v_2) &= (-d_1, d_2, -d_3, -u_1, v_1, -v_2), \\ R_y(d_1, d_2, d_3, u_1, v_1, v_2) &= (-d_1, -d_2, d_3, u_1, -v_1, -v_2), \\ R_{xy}(d_1, d_2, d_3, u_1, v_1, v_2) &= (d_1, -d_2, -d_3, -u_1, -v_1, v_2). \end{aligned} \tag{4.6}$$

We close this section by a theoretical question about invariants. If we want to include higher order terms in (4.1), and hence more terms in (4.4), an algorithm to seek all equivariant maps must be developed. Let Γ be a symmetry group. The problem of determination of all Γ-equivariant maps can be reduced to the determination of the polynomial Γ-equivariant maps, which is a purely algebraic problem [28, 29]. The early work about this area can be traced back from David Hilbert.

Definition 4.7 (Γ-Invariant)**.** *A polynomial $h : \mathbb{R}^n \to \mathbb{R}$ is Γ-invariant if $h(\gamma x) = h(x)$ for all $x \in \mathbb{R}^n$, and $\gamma \in \Gamma$.*

We denote $\mathcal{P}(\Gamma)$ to be the space of all Γ-invariant polynomial.

Definition 4.8 (Hilbert Basis)**.** *The Γ-invariant polynomials $u_1(x), \ldots, u_k(x)$ form a Hilbert basis for $\mathcal{P}(\Gamma)$, if for every $h \in \mathcal{P}(\Gamma)$, there exists a polynomial $p : \mathbb{R}^k \to \mathbb{R}$, such that*

$$h(x) = p(u_1(x), \ldots, u_k(x)).$$

The following theorem shows the finiteness of a Hilbert basis.

Theorem 4.9 (Hilbert-Weyl Theorem)**.** *Let Γ be a compact Lie group acting on a vector space. Then there exists a finite Hilbert basis for the Γ-invariant functions.*

Notice that Hilbert bases are not unique. A Hilbert basis of polynomial invariant functions can be used to characterize any smooth invariant function:

Theorem 4.10 (Schwartz's Theorem)**.** *Let $u_1(x), \ldots, u_k(x)$ be a Hilbert basis for $\mathcal{P}(\Gamma)$. Then for each Γ-invariant C^∞ function $f : \mathbb{R}^n \to \mathbb{R}$ there exists a C^∞ map $p : \mathbb{R}^k \to \mathbb{R}$, such that*

$$f(x) = p(u_1(x), \ldots, u_k(x)).$$

Theorem 4.11 (Poénaru's Theorem)**.** *Let $u_1(x), \ldots, u_k(x)$ be a Hilbert basis and $u(x) = (u_1(x), \ldots, u_k(x))$. There exist Γ-equivariant polynomial mappings $X_1, \ldots, X_l : \mathbb{R}^n \to \mathbb{R}$ such that for each C^∞ Γ-equivariant map $f : \mathbb{R}^n \to \mathbb{R}^n$, there exist C^∞ maps $p_1, \ldots, p_l : \mathbb{R}^k \to \mathbb{R}$ such that*

$$f(x) = p_1(u(x))X_1(x) + \cdots + p_l(u(x))X_l(x)).$$

The simplicity of above theoretical discussion is misleading. In real applications the explicit computations can be too difficult to implement. In our problem the Hilbert basis for T_x, S^1, R_x, and R_y is generated by the following nine invariants

$$s, \quad u_2, \quad I_j = d_j^2 \ (1 \le j \le 3), \quad J = d_1 d_2 d_3, \quad K_1 = d_1 v_2, \quad K_2 = d_2 v_1, \quad K_3 = d_3 u_1,$$

which are not independent but satisfy three relations

$$\begin{aligned} JK_3u_2 + K_1K_2I_3 &= J(sI_3 - J)/4, \\ K_1^2/I_1 + K_2^2/I_2 + K_3^2/I_3 + u_2^2 &= (s^2 - I_1 - I_2 + I_3)/4, \\ J^2 &= I_1I_2I_3. \end{aligned}$$

Therefore theoretically we can have six invariants to generate the set of invariants, or to form a Hilbert basis.

Table 4.1: Invariant subspaces with corresponding isotropy subgroups for the normal form (3.6). Here $[(\alpha,\beta),\gamma] \in T_x \times T_y \times S^1$ and Σ: isotropy subgroups.

Name	Subspace	Generators of Σ
2D invariant subspaces		
TW	$(z,0,0,0)$	$[(\frac{\theta}{p_c},-\frac{\theta}{q_c}),0]$, $[(\frac{\phi}{p_c},\frac{\phi}{q_c}),-\frac{2\phi}{\omega_0}]$
T_xR	$(z,0,0,z)$	$[(\frac{\phi}{p_c},0),-\frac{\phi}{\omega_0}]$, R_y
T_yR	$(z,z,0,0)$	$[(0,\frac{\phi}{q_c}),-\frac{\phi}{\omega_0}]$, R_x
SW	$(z,0,z,0)$	$[(\frac{\pi}{2p_c},\frac{\pi}{2q_c}),-\frac{\pi}{\omega_0}]$, $[(\frac{\theta}{p_c},-\frac{\theta}{q_c}),0]$, R_xR_y
SR	(z,z,z,z)	R_x, R_y
AW	(z,iz,z,iz)	$[R_x(\frac{\pi}{2p_c},-\frac{\pi}{2q_c}),\frac{\pi}{2\omega_0}]$, $[R_y(\frac{\pi}{2p_c},-\frac{\pi}{2q_c}),\frac{\pi}{2\omega_0}]$
4D invariant subspaces		
S_1	(z_1,z_2,z_1,z_2)	R_xR_y
S_{13}	$(z_1,z_2,0,0)$	$[(0,\frac{\phi}{q_c}),-\frac{\phi}{\omega_0}]$
S_{12}	$(z_1,0,0,z_2)$	$[(\frac{\phi}{p_c},0),-\frac{\phi}{\omega_0}]$
S_{23}	$(z_1,0,z_2,0)$	$[(\frac{\pi}{2p_c},\frac{\pi}{2q_c}),-\frac{\pi}{\omega_0}]$, $[(\frac{\theta}{p_c},-\frac{\theta}{q_c}),0]$
S_{2+}	(z_1,z_1,z_2,z_2)	R_x
S_{2-}	(z_1,iz_1,z_2,iz_2)	$[R_x(\frac{\pi}{2p_c},-\frac{\pi}{2q_c}),\frac{\pi}{2\omega_0}]$
S_{3+}	(z_1,z_2,z_1,z_2)	R_y
S_{3-}	(z_1,iz_2,z_2,iz_1)	$[R_y(\frac{\pi}{2p_c},-\frac{\pi}{2q_c}),\frac{\pi}{2\omega_0}]$

4.3 2D and 4D Invariant Subspaces

In this section we analyze basic wave solutions, 2D subspaces of (4.1), and their creation in primary and secondary bifurcations for general θ and a_j from 4D invariant subspaces, and relate them to to basic solutions of (3.6) in the limit $\theta \to 0$.

If we translate a general pattern in y-direction, the resulting pattern, $T_y(z_1,z_2,z_3,z_4)^T$, is governed by different translated amount of y-values up to π/q_c in (4.1). This fact results from the y-translation symmetry breaking effect. If such a symmetry is preserved, as in the normal form (3.6), T_y-conjugate patterns follow the same dynamics.

Table 4.1 provides isotropy subgroups of all subspace for the normal form [49, 57, 23], which can be used to search thoroughly which subspaces are invariant for (4.1). Notice that only the 2D subspaces T_xR, SR, and the 4D subspaces S_{3+}, S_{12}, S_{2+}, S_1 of Table 4.1 do not contain the element T_y in their isotropy subgroups, Therefore,

only these subspaces (S_{3+}, S_{12}, S_{2+}, S_1, T_xR, SR) are invariant in (4.1).

We study the dynamics in S_{3+} first. In the normal form (3.6) there is a family of solutions in S_{3+}, $(e^{i\beta}z_1, e^{i\beta}z_2, e^{-i\beta}z_2, e^{-i\beta}z_1)$, with arbitrary phase variable β. Due to the symmetry breaking, the freedom of choosing β is no longer there, and only $\beta = k\pi/2$ are allowed, where k is any integer. Therefore, the phase pinning occurs in S_{3+}, resulting in two S_{3+} copies, the "plus"-copy $S^+_{3+} = (z_1, z_2, z_2, z_1)$ and the "minus"-copy $S^-_{3+} = (z_1, z_2, -z_2, -z_1)$. The dynamics of (4.1) restricted on these two copies of subspace S_{3+} is described by the normal form for a Hopf bifurcation with $\mathbb{O}(2)$-symmetry,

$$\begin{aligned} \dot{z}_1 &= (a_0 \pm \theta + A|z_1|^2 + B|z_2|^2)z_1, \\ \dot{z}_2 &= (a_0 \pm \theta + A|z_2|^2 + B|z_1|^2)z_2, \end{aligned} \tag{4.12}$$

with A, B given in Table 3.1(b), the plus or minus signs are determined by the $\pm$ sign of $S^{\pm}_{3+}$. The remaining unbroken symmetries act in this subspace as

$$\begin{aligned} T_x: &\quad (z_1, z_2) \rightarrow (e^{ip_c x_0}z_1, e^{-ip_c x_0}z_2), \\ R_x: &\quad (z_1, z_2) \rightarrow (z_2, z_1), \\ T_t: &\quad (z_1, z_2) \rightarrow e^{i\omega_c t_0}(z_1, z_2), \end{aligned} \tag{4.13}$$

and R_y acts trivially. This system has three types of solutions: the trivial solution, $z_1 = z_2 = 0$, with eigenvalues $a_{0r} \pm \theta_r$ and $a_{0r} \pm \theta_r$; the traveling wave solution, $(z_1, z_2) = (z, 0)$ or $(0, z)$, with eigenvalues $-2(a_{0r} \pm \theta_r)$ and $(a_{0r} \pm \theta_r)(A_r - B_r)/A_r$; and the standing wave solution $z_1 = z_2 \neq 0$ with eigenvalues $-2(a_{0r} \pm \theta_r)$ and $2(a_{0r} \pm \theta_r)(B_r - A_r)/(A_r + B_r)$. The system (4.12) is well studied. All other solutions are transient. The derivation of basic wave solutions, bifurcation diagrams, and stability properties can be found in [29].

Restricting (4.1) to the subspaces S_{12} and S_{2+} results in

$$\begin{aligned} \dot{z}_1 &= (a_0 + A|z_1|^2 + B|z_2|^2)z_1 + \theta z_2, \\ \dot{z}_2 &= (a_0 + A|z_2|^2 + B|z_1|^2)z_2 + \theta z_1. \end{aligned} \tag{4.14}$$

On the subspace S_{12}, R_x maps S_{12} to its conjugate copy $(0, z_1, z_2, 0)$, so reflection over x does not hold within the invariant subspace S_{12}. The other inherited unbroken group actions are

$$\begin{aligned} T_x: &\quad (z_1, z_2) \rightarrow (e^{ip_c x_0} z_1, e^{ip_c x_0} z_2), \\ R_y: &\quad (z_1, z_2) \rightarrow (z_2, z_1), \\ T_t: &\quad (z_1, z_2) \rightarrow e^{i\omega_c t_0}(z_1, z_2), \end{aligned} \tag{4.15}$$

Notice that T_x and T_t act in the same way, which implies that translation of patterns in S_{12} along x-direction by x_0 is equivalent to the overall phase shift by $p_c x_0$. On the subspace $S_{2+} = (z_1, z_1, z_2, z_2)$, T_x does not hold within S_{2+}, since it maps S_{2+} to a continuous family of conjugate copies. R_x acts trivially, while

$$\begin{aligned} R_y: &\quad (z_1, z_2) \rightarrow (z_2, z_1), \\ T_t: &\quad (z_1, z_2) \rightarrow e^{i\omega_c t_0}(z_1, z_2). \end{aligned} \tag{4.16}$$

System (4.14) is the four dimensional normal form for a Hopf bifurcation with broken translation symmetry due to θ-terms. Similar setups are analyzed in [20, 35, 31]. Dangelmayr and Knobloch in [20] have pointed out that the translation symmetry breaking terms split the eigenvalues, which are of multiplicity two in the perfect symmetric case (4.12), into two pairs, selecting two standing waves with phase difference by π, i.e. (z, z) and $(z, -z)$. We denote by $\theta = \epsilon \exp(i\alpha)$, $B - A = p \exp(i\gamma)$, $r^2 = x_1^2 + x_2^2$, and $\beta = \alpha - \gamma$. One standing wave, (z, z), bifurcates from the trivial solution if $a_{0r} \geq -\epsilon \cos\alpha$, then is followed by a perturbed version TW at a secondary bifurcation when $pr^2 \cos\beta + 2\epsilon = 0$; the other standing wave, $(z, -z)$, is generated from the primary bifurcation at $a_{0r} = \epsilon \cos\alpha$ and followed by the perturbed TW

resulting from a secondary bifurcation when $pr^2\cos\beta - 2\epsilon = 0$. This scenario is confirmed by our numerical simulations, described in the next section.

In the subspace S_1 the system (4.1) is reduced to

$$\begin{aligned} \dot{z}_1 &= (a_0 + A|z_1|^2 + B|z_2|^2)z_1 + a_5\overline{z}_1 z_2^2 + \theta z_2, \\ \dot{z}_2 &= (a_0 + A|z_2|^2 + B|z_1|^2)z_2 + a_5\overline{z}_2 z_1^2 + \theta z_1. \end{aligned} \tag{4.17}$$

The group actions T_x result in a continuous family of conjugate copies of S_1, and the other actions are

$$\begin{aligned} R_x: &\quad (z_1, z_2) \rightarrow (z_2, z_1), \\ R_y: &\quad (z_1, z_2) \rightarrow (z_2, z_1), \\ T_t: &\quad (z_1, z_2) \rightarrow e^{i\omega_c t_0}(z_1, z_2). \end{aligned} \tag{4.18}$$

Notice that R_x and R_y act in the same way on S_1, i.e., the reflection about x is equivalent to reflection about y. The system is equivariant under (4.18); $\theta = 0$ in (4.17) corresponds to the normal form of a Hopf bifurcation with D_4-symmetry [51]. The nonzero θ breaks the $\mathbb{Z}_4$-symmetry, a subgroup of $\mathbb{D}_4$, down to $\mathbb{Z}_2$.

To study bifurcations on S_1, we use symmetry-adapted variables (4.3). Restricting the dynamical system (4.4) on S_1 leads to $d_2 = d_3 = u_1 = v_1 = 0$, and the dynamics of the nonzero symmetry-adapted variables follows

$$\begin{aligned} \dot{d}_1 &= 2a_{0r}d_1 + b_{01}sd_1 + 4a_{5i}u_2v_2 + 4\theta_i v_2, \\ \dot{s} &= 2a_{0r}s + (b_0 s^2 + b_1 d_1^2)/2 + 2a_{5r}(u_2^2 - v_2^2) + 4\theta_r u_2, \\ \dot{u}_2 &= 2a_{0r}u_2 + \alpha_2 s u_2 - \beta_2 d_1 v_2 + \theta_r s, \\ \dot{v}_2 &= 2a_{0r}v_2 + \alpha_1 s v_2 + \beta_1 d_1 u_2 - \theta_i(d_1 + d_3) \end{aligned} \tag{4.19}$$

Two copies of SR, $SR^{\pm} = (z, \pm z)$, can be written as fixed points on (4.19) as $s = \pm u_2 = -2(\pm\theta_r + a_{0r})/\alpha_2$, and $d_1 = v_2 = 0$. The primary bifurcations of SR are

determined by the eigenvalues of the matrix

$$\begin{pmatrix} 2a_{0r} + b_{01}s & 4a_{5i}u_2 + 4\theta_i \\ \beta_1 u_2 - \theta_i & 2a_{0r} + \alpha_1 s \end{pmatrix},$$

and $4(-b_0\theta_r + a_{0r}a_{5r})/(b_0 + a_{5r})$ for SR^+, or $4(b_0\theta_r + a_{0r}a_{5r})/(b_0 + a_{5r})$ for SR^-. The secondary bifurcation is hard to analyze compared to (4.14) due to no closed analytic form for TW. Notice that, in the normal form with T_y symmetry, there are two conjugate copies of AW: $AW^+ = (iz, z)$ and $AW^- = (z, iz)$, and two conjugate copies of SW: $SW^+ = (z, 0)$ and $SW^- = (0, z)$. Moreover, $d_1 = u_2 = 0$, $s = \pm v_2 = -2a_{0r}/\alpha_1$ for $AW^\pm$, and $u_2 = v_2 = 0$, $s = \pm d_1 = -2a_{0r}/b_{01}$ for $SW^\pm$. When symmetry-breaking effect slowly increases from zero, we get perturbed versions of $AW^\pm$ and $SW^\pm$, which are continuous variations of the perfect symmetry copies. After some critical values, the perturbed basic patterns jump abruptly to SRs, which are characterized by $d_1 = v_2 = 0$. These scenarios are shown in Figure 4.2, where the parameters are chosen in (3.11) with $a_{3r} = -0.6442$, which correspond to the Feigenbaum accumulation point (see [18]).

Notice that R_x, R_y, and R_{xy} in (4.6) determine three fixed point spaces, $\mathrm{Fix}(R_x)$, $\mathrm{Fix}(R_y)$, and $\mathrm{Fix}(R_{xy})$, and $S_{2+} \subset \mathrm{Fix}(R_x)$, $S_{3+} \subset \mathrm{Fix}(R_y)$, and $S_1 \subset \mathrm{Fix}(R_{xy})$. We can consider these fixed point subspaces for symmetry adapted variables to be the generalized versions of 4D invariant subspaces.

For 2D invariant subspaces, there exist two copies of T_xR and SR up to conjugacy due to two copies of S_{3+}, which are $T_xR^\pm = (z, 0, 0, \pm z)$ and $SR^\pm = (z, z, \pm z, \pm z)$. Compared to (3.9) the differential equation for the complex variable z is

$$\dot{z} = (a_0 \pm \theta + c|z|^2)z, \tag{4.20}$$

where the $\pm$ is determined by whether it is a "+" or "−" copy of $T_xR^\pm$ or $SR^\pm$.

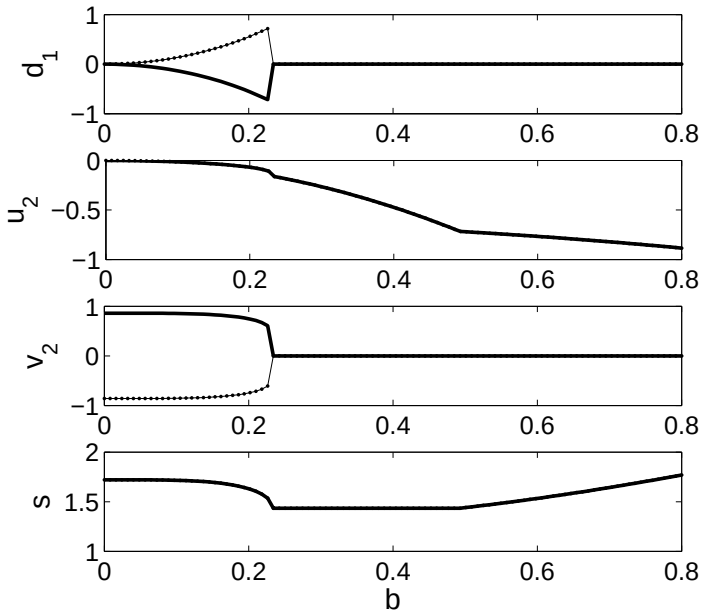

(a)

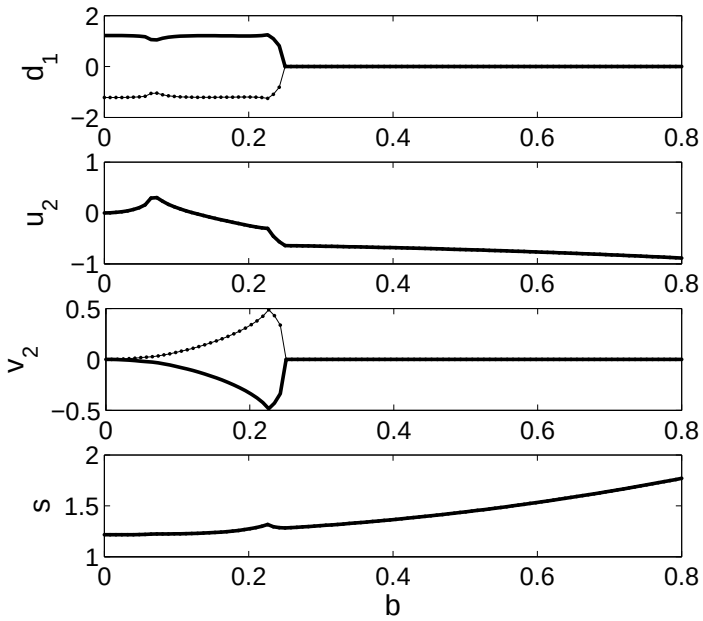

(b)

Figure 4.2: (a) Existence of AW for small symmetry-breaking effects. (b) Existence of SW for small symmetry-breaking effects. Solid lines stand for $AW^+ = (iz, z)$ in (a) and $SW^+ = (z, 0)$ in (b) and dotted lines for $AW^- = (z, iz)$ in (a) and $SW^- = (0, z)$ in (b). Symmetry-breaking effect parameter $\theta = (a_4 + a_5)|b|^2$. Here symmetric $AW^{\pm}$ is characterized by $d_1 = u_2 = 0$ and $SW^{\pm}$ by $u_2 = v_2 = 0$.

To sum it up, T_xR and SR can be created from primary Hopf bifurcations in (4.1). Other basic patterns in Table 3.1(a) can come out as perturbed versions from secondary bifurcations for small symmetry breaking effects, i.e. small θ-values.

4.4 Complex Dynamics of the Perturbed Normal Form

4.4.1 Overview

In this numerical study we vary the symmetry breaking parameter b and fix the normal form parameters chosen in (3.11), The value $a_{3r} = -0.6442$ corresponds to the Feigenbaum accumulation point (see [18]). The similar behaviors are found for a range of $-a_{3r}$ close to 0.6442. b changes in the range

$$0 \leq b \leq 0.8.$$

The following two main regions are distinguished based on their important dynamic characteristics:

$$\begin{aligned} \text{Region I} &: 0 \leq b \leq 0.306, \\ \text{Region II} &: 0.306 < b \leq 0.8. \end{aligned}$$

The features of both regions are given in Figure 4.3. The Region I is characterized by alternations between chaos and periodic windows. It starts with period doubling up to $b = 0.004$, then undergoes symmetry and decreasing, followed by bistability with two qualitatively different periodic orbits. These two orbits evolve to chaos independently and cause crisis-induced intermittency at $b = 0.0642027$. Just one of them survives after intermittency. Between $b = 0.0648$ and $b = 0.144$ there exists a number of chaos and periodic windows, without showing any dynamics we want to focus in this paper. At $b = 0.144$, switching between symmetry-conjugated chaotic saddles,

another crisis-induced intermittency, takes place, which is similar to the switching in GCCGLEs (2.11) (Figure 3.2).

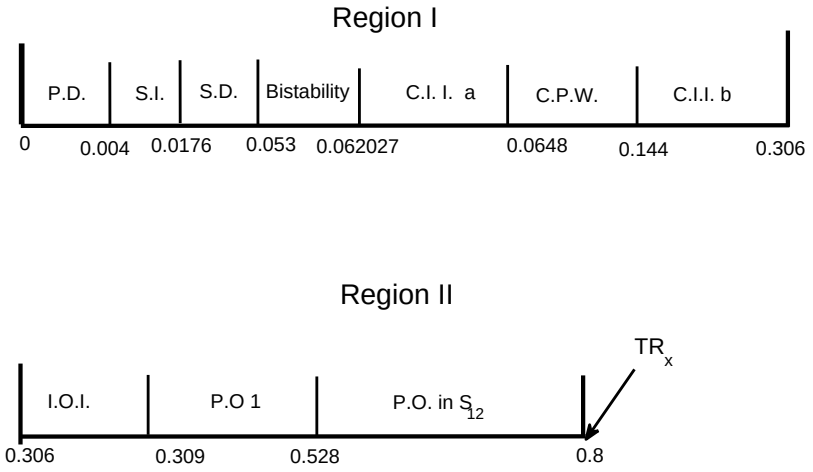

Figure 4.3: Characteristics of region I and II. P.D.: period doubling. S.I: symmetry increasing. S.D: symmetry decreasing. C.I.I. a and b: crisis-induced intermittency a and b. C.P.W.: chaos and periodic windows. I.O.I.: in-out intermittency. P.O. 1: periodic orbit in the generalized subspace S_1.

The region II is composed of a variety of transitions among different periodic orbits. Periodic Orbit I appears after in-out intermittency, which lasts between $b = 0.306$ and $b = 0.309$. We notice that in-out intermittency disappears as transient chaos. Periodic orbit I is characterized by $r_1 = r_3$, $r_2 = r_4$, and $\zeta = \eta$, which is in the invariant subspace $\mathrm{Fix}(R_{xy})$, a generalized version of S_1.

At $b = 0.528$ the fixed point subspace $\mathrm{Fix}(R_{xy})$ loses the transverse stability, and the periodic orbit I is replaced by the periodic orbit II in the 4D subspace S_{12}, whose dynamics is governed by (4.14). The system (4.14) is analyzed in detail in [20]. The translation symmetry breaking terms split the eigenvalues of the Jacobian matrix with eigenvalues of multiplicity two in the $O(2)$-symmetric case into two pairs. One pair of eigenvalues corresponds to the traveling rectangle $(z, 0, 0, -z)$, TR_x, which occurs here at $b = 0.8$. The other one corresponds to the traveling rectangle $(z, 0, 0, z)$, which

does not show up for the range of parameters in this study.

In the following subsections, we will focus on the switching intermittency, defined as crisis-induced intermittency in [15, 13], and in-out intermittency, which are unique in the perturbed normal form. Then we will describe other dynamic phenomena, such as symmetry increasing and decreasing, bistability, which are qualitatively similar to behaviors found in the normal form [18]. We modify projective coordinates in (3.12) to

$$D_j = d_j/s(1 \leq j \leq 3), \quad U_k = u_k/s, \quad V_k = v_k/s(1 \leq k \leq 2),$$

in order to make comparison with [18], and emphasize symmetric properties by normalizing variables.

4.4.2 Crisis-induced Intermittency

Crisis is the event of sudden qualitative changes in chaotic attractors as a system parameter passes through a critical value, which is first proposed in [14]. The mechanism of a crisis is a collision between a chaotic attractor and a coexisting unstable manifold, usually an unstable periodic orbit or an unstable fixed point.

Authors in [14] use the following elementary quadratic map to illustrate the crisis phenomenon

$$x \longmapsto C - x^2. \tag{4.21}$$

The bifurcation diagram of the map (4.21) is provided in Figure 4.4. When $C < -1/4$, all orbits with any initial conditions move to $x = -\infty$, because no fixed point exists. A saddle-node bifurcation happens at $C = -1/4$, from which a stable and an unstable fixed point are generated. In Figure 4.4, the unstable fixed point is denoted by the dashed curve, and the stable one is denoted by solid curve. We can compute the

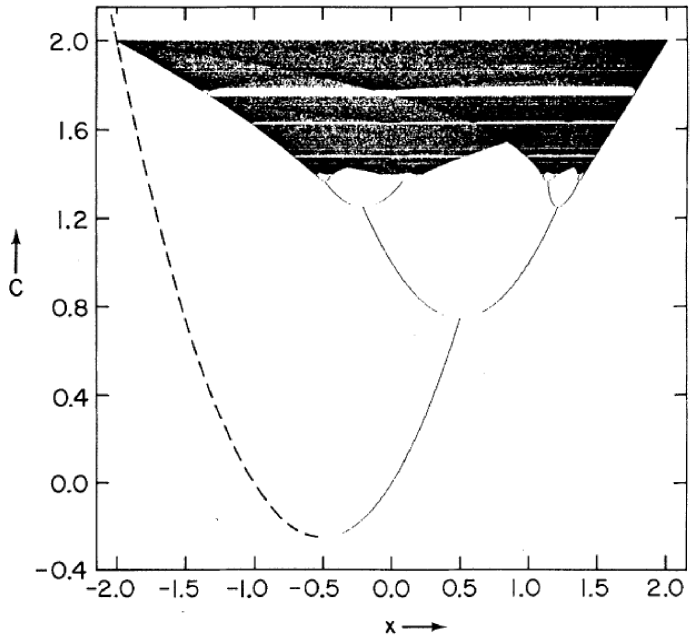

Figure 4.4: Bifurcation diagram for the map (4.21), from [14]. The dashed line is the unstable fixed point.

dashed curve from

$$x = -x^* = -\frac{1}{2} - \sqrt{\frac{1}{4} + C}, \quad \text{for } C \geq -\frac{1}{4}.$$

As C is increased past $-1/4$, the stable fixed point goes through the period doubling, leading to chaos [27]. Figure 4.4 indicates that for $1/4 \leq C \leq 2$, and for any initial point in the range $|x| < x^*$, the orbit of the map (4.21) is bounded, and orbits initialized in $|x| > x^*$ go to $x = -\infty$. Therefore $|x| < x^*$ is the basin of attraction for the bounded orbits. Notice that at $C = 2$, the chaotic band intersects with the unstable point $x = x^*$, then the chaotic attractor is destroyed. This type of crisis occurs on the boundary of the basin. Therefore we call it a boundary crisis, which lead to a destruction of the attractor and its basin. Transient chaos can be obtained for C slightly bigger than 2. If the initial condition is in the region which was chaotic for C slightly less than 2, one can observe orbits initially attracted to the former

chaotic attractor like for $C < 2$. After chaotically moving around for a long time, the orbits move to some other distant attractor. The length of the transient chaos is very sensitive to the initial conditions. However, if we have many randomly chosen initial conditions, the average lifetime of the transient chaos can be computed. The relation between the average lifetime of transient chaos and a system parameter is well studied in [16, 13], from which the concept of the critical exponent of the transient chaos is proposed.

The collision between the chaotic attractor and the unstable orbit can occur within the basin of attraction, which is called an interior crisis, leading to sudden widening of a chaotic attractor. Figure 4.5 provides such an example, which is an enlargement of bifurcation diagram of the map (4.21) between 1.72 and 1.82. The dashed lines correspond to unstable period-three orbits created from the saddle-node bifurcation. Notice that for a certain range of C less than a critical value, chaos occurs in three different bands. But when C is slightly bigger than the critical value, the three chaotic regions suddenly widen to form a single band. Then for an orbit initialized in one of these three former chaotic bands, at the beginning it moves around in a chaotic manner, cycling between the three regions, as if C is below the critical value. After a relatively long time, the orbit suddenly moves out of the old region and goes to a formerly empty region, which is available after the interior crisis. Then it returns to the old region for a while followed by another return into a new region, and so on. This type of random alternation between two dynamical behavior is called crisis-induced intermittency [13].

Notice that such dynamics in the map (4.21) is very representative for a class of nonlinear maps, as the well-known logistic map

$$x \longmapsto rx(1-x).$$

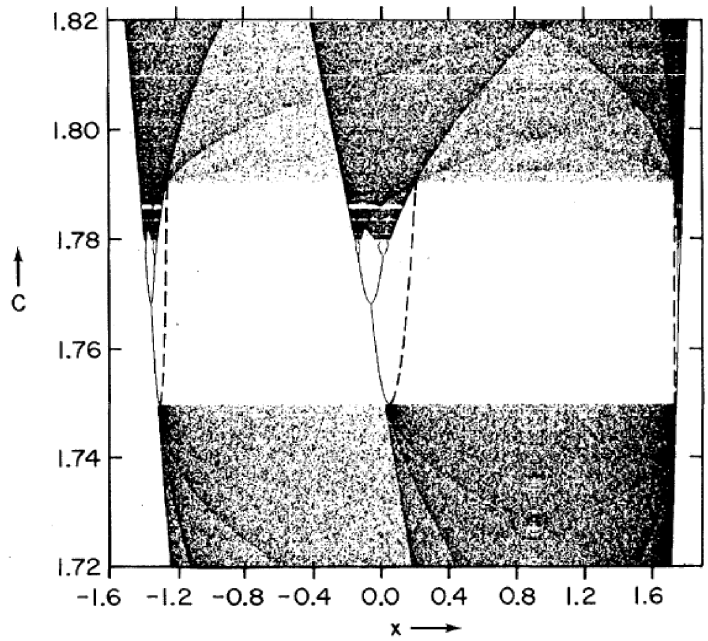

Figure 4.5: Zoom in the bifurcation diagram of the map (4.21) in the period-three saddle-node bifurcation, from [14]. The dashed lines denote the unstable period-three orbit generated from the tangent bifurcation.

The map (4.21) becomes the logistic map by the following linear transform

$$x \longmapsto \frac{1}{r}x + \frac{1}{2}.$$

The relation between the parameter r in the logistic map and C in the quadratic map (4.21) is

$$2r + 4C = 1.$$

There is another type of crisis, which leads to attractor mergings. Suppose there exist two chaotic attractors with a common boundary, which is an unstable manifold, separating their basins of attraction. If symmetries are imposed in the dynamical system, like in the case of the perturbed normal form (4.1), these two chaotic attractors could enlarge and touch the basin boundary simultaneously at the crisis, as the system parameter increases and passes through the critical value. Then a single

chaotic attractor is formed as a result of the attractor merging. Intermittent switching occurs. For the system parameter slightly greater than the critical value, an orbit will spend a long stretch of time in the region of one of the former attractors. After such a time stretch, the orbit abruptly exists this region, and then spends a long stretch of time in the region of the other former attractor, and so on. The mean time between switches, τ, is important in the study of this dynamics. It is proved in [13] that τ can be written as a function of bifurcation parameter b as $\tau \propto |b-b_c|^{-\gamma}$, where γ is the critical exponent.

Figure 4.1 provides us one example of such switching intermittency from the low dimensional system (4.1), which is of great interest since it is qualitatively similar to simulations of the high dimensional Ginzburg Landau system (Figure 3.2). Here we choose projective symmetry-adapted variables (3.12) to distinguish two symmetry-conjugate copies, one corresponding to the positive band of D_3, the other corresponding to the negative band of D_3. Simulations demonstrate that switching behavior starts after $b = 0.144$, pauses at $b = 0.166$, and resumes at $b = 0.199$. Because of symmetries (4.6) in the perturbed normal form (4.1), below the critical parameter b_c there exist two symmetry-conjugated chaotic attractors, shown in the first two panels of Figure (4.6). Just past b_c these is one big chaotic attractor resulting from the chaotic attractor merging. Then the frequency of switchings becomes faster and faster as the system parameter b increases, until we cannot distinguish these two symmetrically conjugate copies, as shown in the case at $b = 0.28$ (Figure 4.7(a)). The reason of this switching dynamics is that conjugate attractors collide with unstable invariant sets on the boundaries of their basins simultaneously at the crisis due to the symmetry. Then the unstable submanifold of one pre-crisis chaotic attractor connects with the stable submanifold of the conjugate one to form a heteroclinic orbit. We estimate the mean time between switches, τ, versus different parameter values, b, to establish the power law $\tau \propto |b - b_c|^{-\gamma}$. Figure 4.7(b) indicates that γ can be approx-

imated to be 3.9235 in this case. Other models exhibiting the similar switching, such as the double-well potential system, can be found in [33, 13].

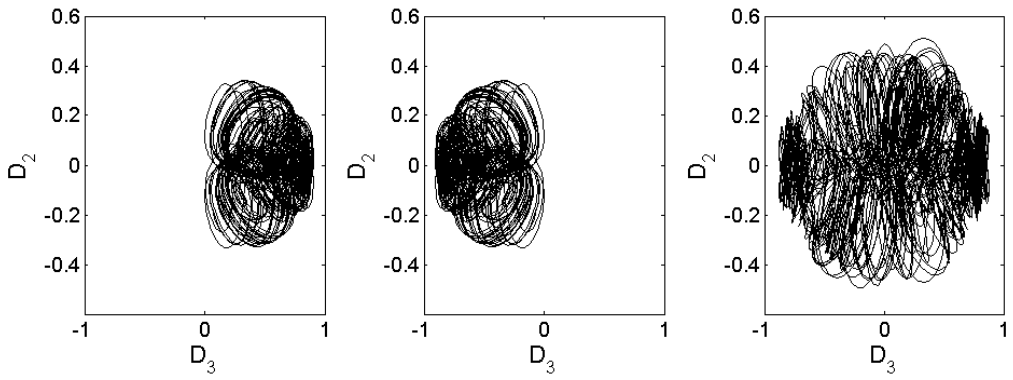

Figure 4.6: Phase plots of (4.1) for $b = 0.198 < b_c$ (the first two panels) and $b = 0.2 > b_c$ (the third panel).

4.4.3 In-Out Intermittency and Transient Chaos

In-out intermittency follows the switching intermittency in the previous subsection. Detailed description regarding in-out intermittency is presented in Section 3.4, where the invariant manifold (the normal form) is obtained by ignoring spatial variations in Ginzburg Landau system (2.11). In this subsection we provide an example of in-out intermittent behavior relative to an invariant subspace forced by symmetries, followed by transient chaos and a periodic orbit.

The symmetry R_{xy} in (4.6) for the perturbed normal form (4.1) induces an invariant subspace $\mathrm{Fix}(R_{xy})$, i.e. $d_2 = d_3 = u_1 = v_1 = 0$. It is easy to check that b in the system (4.4) is a non-normal parameter, since its variation changes the dynamics inside the invariant subspace $\mathrm{Fix}(R_{xy})$ as well as the one outside it. When the value of b gets closer to $b = 0.306$, (which is the continuation of Figure 4.7(a)), the chaotic behavior in d_2, d_3, u_1, and v_1 is interrupted by regular zero-value phases. After transient chaos for $b \geq 0.309$, $\mathrm{Fix}(R_{xy})$ becomes stable in the transverse direction. Therefore a periodic orbit residing in this subspace becomes stable in the full

system (4.4). Time series of d_3 at $b = 0.308$ are provided in Figure 4.8; d_2, u_1, and v_1, which are not included in Figure 4.8, demonstrate similar behaviors. Extreme values of s, denoted by s_e in the last panel of Figure 4.8, imply periodic phases for dynamics near the invariant subspace. We confirm it is not on-off intermittency [30, 44, 56], because on-off cases require chaos within the invariant subspace, normal parameters, and skew-product, which are absent in our model. The variances of d_3 within each 10-time units are used in the third panel of 4.8 to distinguish in and out phases.

Authors in [5] use a Markov chain model to investigate in-out intermittency and derive its statistics. Here we use the least square method to compute the scaling law (Figure 4.9), $P_\tau \sim \alpha n^{-3/2} e^{-\beta n} + \gamma e^{-\delta n}$, where τ is the mean time between bursts, P_τ is the distribution of τ, $n = 0.1\tau$, $\alpha = 0.3321$, $\beta = 0.0524$, $\gamma = 0.0156$, and $\delta = 0.0506$. The exponent $-3/2$ is from the similarity between a Brownian motion and a chaotic walk [30]. The heavy shoulder caused by $\gamma e^{-\delta n}$ in Figure 4.9 is another feature distinguishing in-out and on-off cases.

Transient chaos is observed during the process of disappearance of in-out intermittency in Figure 4.8. Figure 4.10 shows how the length of transients varies with the system parameter b with fixed initial conditions. If we want to establish a scaling law about the relation between the average length and the parameter, a large number of initial conditions should be chosen to compute the mean length of transients.

Transient chaos is a common dynamical behavior when there exists an unstable chaos. One famous example of transient chaos is the Lorenz system in a certain range of parameter r, while other parameters are fixed [50]. Authors in [34, 59] point out that when a symmetric homoclinic orbit for the origin is formed at $r \approx 13.96$, chaos is born but not attracting. Since there are two other symmetry-related stable fixed point on the positive and negative x-axis, for any orbit we can see transient chaos initially, as dynamics within the Lorenz chaotic attractor, then it moves to one of these two fixed points. At $r \approx 24.06$, the transient chaos is converted into a chaotic

attractor. Ott [43] attributed this to crisis. In Section 4.4.2 we mentioned that a boundary crisis can destroy a chaotic attractor and lead to transient chaos. If we change parameter in the other direction, we can convert the transient chaos into a chaotic attractor.

Transient chaos occurring in the Figure 4.10 seems to be created from the increasing stability in the transverse direction of the invariant subspace as the system parameter varies, not from a crisis. Further theoretical work needs to be developed to prove this claim.

4.4.4 Symmetry Increasing and Decreasing, Bistability

The phenomena of symmetry increasing, symmetry decreasing and bistability are not novel in the perturbed normal form (4.1). The qualitatively similar dynamics also shows up in the normal form (3.6) [18].

Authors in [10, 9] introduce the concept of symmetry-increasing bifurcation to understand and analyze the dynamics of symmetries in chaotic systems. Suppose the group Γ is the symmetry group for a dynamical system acting on the phase space. Assume A_λ to be an attractor depending on the system parameter λ, and Σ_λ to be the symmetry of the attractor A_λ, i.e.,

$$\Sigma_\lambda = \{\lambda \in \Sigma : \ \lambda A_\lambda = A_\lambda\}.$$

A symmetry-increasing bifurcation occurs at $\lambda = \lambda_0$ if

1. $\Sigma_\lambda = \Sigma_1$, for $\lambda < \lambda_0$.

2. $\Sigma_\lambda = \Sigma_2$, for $\lambda > \lambda_0$.

3. $\Sigma_1 \subset \Sigma_2$.

If the parameter λ varies in the opposite direction, we call it a symmetry-decreasing

bifurcation. A variety of examples are provided in [10]. One simple example is the odd-logistic equation

$$x \longmapsto f(x, \lambda) = \lambda x - x^3, \tag{4.22}$$

with the symmetry $\mathbb{Z}_2 = \{1, \rho\}$ acting by $\rho x = -x$. When $\lambda < 1$, the only stable fixed point is $x = 0$. The pitchfork bifurcation occurs at $\lambda = 1$, leading to two stable symmetry conjugate fixed points and one unstable fixed point, $x = 0$. Figure 4.11 provides bifurcation diagram for the positive fixed point. These two symmetry conjugate fixed points undergo a period-doubling cascade, resulting in a pair of symmetry conjugate chaotic attractors. At $\lambda_c = 3\sqrt{3}/2$ these two chaotic attractors merge into a $\mathbb{Z}_2$-symmetric attractor. Notice that a symmetry-increasing bifurcation is often called switching intermittency induced by crisis which is described in Section 4.4.2, when the average time between switches is studied.

In other situations the symmetry of an attractor varies continuously with the system parameter without a sudden change, like symmetry-increasing in the normal form [18] and in the perturbed normal form, which will be described later. The concept of symmetry detectives has been developed to deal with these cases in [6]. Dangelmayr in [18] uses the normalized asymmetry measure

$$M = |\sum_{i=0}^{N-1} X(i)| / \sum_{i=0}^{N-1} |X(i)|$$

to investigate the symmetry variation of X about $X = 0$. A fully asymmetric orbit, which means no sign changes of X, would have $M = 1$. A perfectly symmetric attractor has $M = 0$.

Symmetry increasing and decreasing take places repeatedly for the whole range of b-values in the perturbed normal form (4.1). Figure 4.12 provides examples where b is between 0 and 0.0524. When b is progressing from 0, it is the continuation of symmetry decreasing of P_{1a} in [18]. The orbit undergoes period doubling as b increases

from 0 to 0.004, where we can see that the chaotic bands in phase portrait become thicker as b is increasing (Figure 4.12(a) upper left and right). The lower left panel in Figure 4.12(a) illustrates that a symmetric periodic orbit show up at $b = 0.0139$, which is P_{1s}in [18]. This scenario, and simulations for nearby $-a_{3r}$s (not included here), imply that weak symmetry-breaking terms take dynamics back to the normal form, P_{1s}, a symmetric periodic orbit outside subspace S_1. As b increases further, the symmetry in P_{1s} is broken, and symmetry breaking takes place (Figure 4.12(a) lower right).

Two qualitatively different periodic orbits follow, i.e., bistability. Both stable orbits, one symmetric and the other asymmetric, are stable for corresponding attraction basins (upper left of Figure 4.12(b) and (c)). On one hand, Figure 4.12(b) (upper right and lower left) illustrates that the asymmetric periodic orbit first undergoes period doubling to chaos. Then after critical value $b = 0.0594$, an intermittent switching takes a place behaviors in D_2-component, which alternates back and forth between a pair of conjugate chaotic manifolds. On the other hand, the symmetric periodic orbit encounters symmetry decreasing (Figure 4.12(c) upper right), period doubling (Figure 4.12(c) lower left), and finally symmetric increasings to become a symmetric chaotic attractor (Figure 4.12(c) lower right). The time series in Figure 4.13 describes dynamics in the lower right panels of Figure 4.12 (b) and (c), which shows these two chaotic state are qualitatively different. By the end the asymmetric chaos replaced by the symmetric one through crisis.

4.4.5 A New Type of Intermittency

A new type of intermittency is found during the process of symmetry increasing, as shown at $b = 0.0125$. Intermittency takes place between symmetric chaos (lower left panel in Figure 4.14(a)) and a pair of conjugate asymmetric chaos (lower right in Figure 4.14(a)). Time series is provided in the upper panel of Figure 4.14(b).

The more chaotic pieces in the time series correspond to the symmetric chaos. To investigate this type of time series further, we discretize data by the following Poincaré map:

$$\dot{D}_3 = 0, \quad \ddot{D}_3 < 0,$$

which is denoted as $D_3(n)$ in the lower panel of Figure 4.14(b). The iterates $D_3(n+1)$ versus $D_3(n)$ is provided in lower right panel of Figure 4.14(a). The symmetric chaos corresponds to a unimodal map, and each asymmetric chaos corresponds to that pair of leaves above the unimodal map. The pair of leaves forms a tunnel. An orbit enters this tunnel from the top entrance, moves chaotically through the tunnel, and leaves it from the bottom exit. Then this orbit follows the unimodal chaotic map until it moves to the top entrance of the tunnel again. Therefore we see intermittency between two different chaotic phases. As far as we know, this is a new type of intermittency, which has not been investigated yet in the literature. It is the future work to study characteristics of this type of intermittency and to construct some simple nonlinear map with such dynamics.

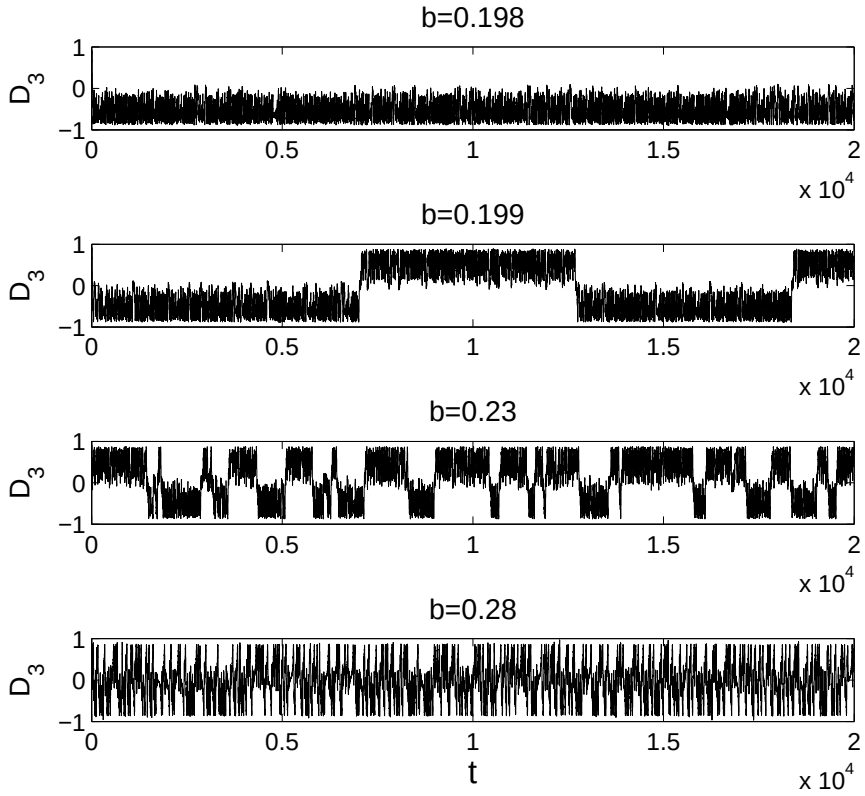

(a)

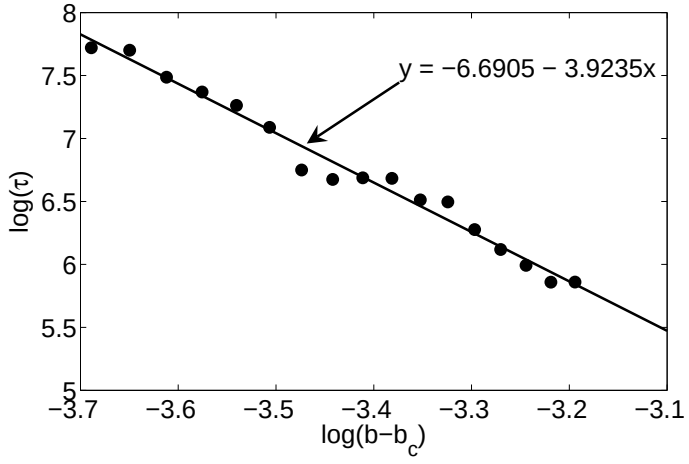

(b)

Figure 4.7: One example of crisis-induced intermittency. (a): Time series of switching D_3 under different b-values. (b): $\log \tau$ vs $\log(b - b_c)$. τ is the mean time between switches. b_c is the critical value for switching intermittency, which is estimated to be 0.199.

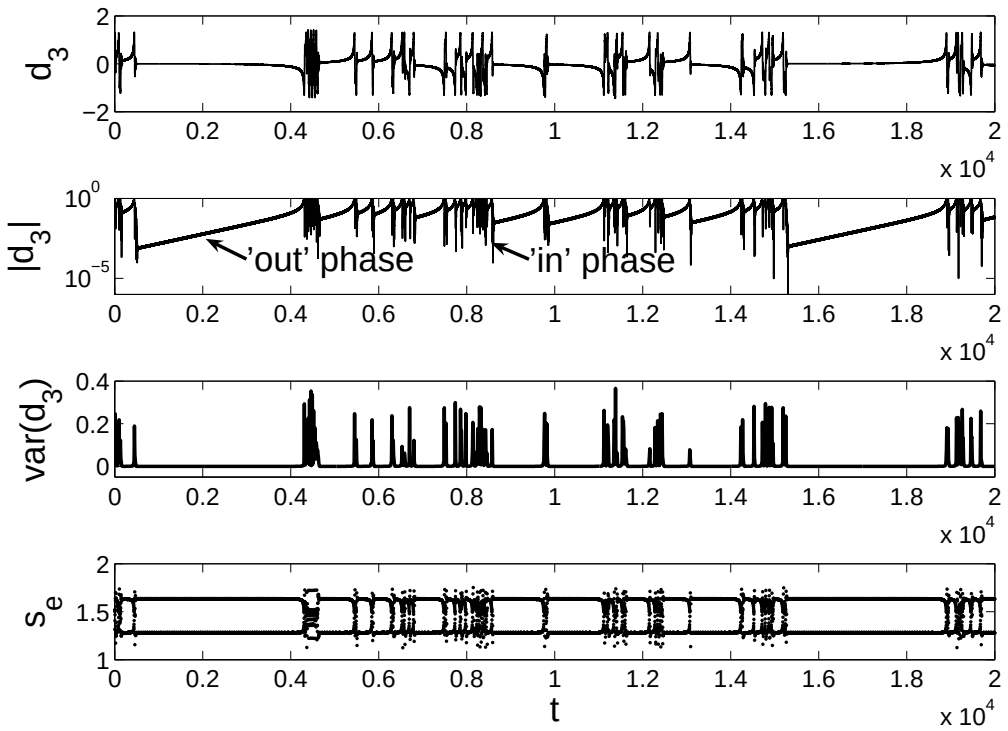

Figure 4.8: Time series of (4.1) for in-out intermittency at $b = 0.308$. Note the second panel is in the log scale. d_2, u_1, and v_1, show similar behaviors as d_3 (not included). The third panel shows the variance of d_3 within each 10-time units. The last panel demonstrates extreme values of s, s_e, indicating a periodic orbit near the invariant subspace.

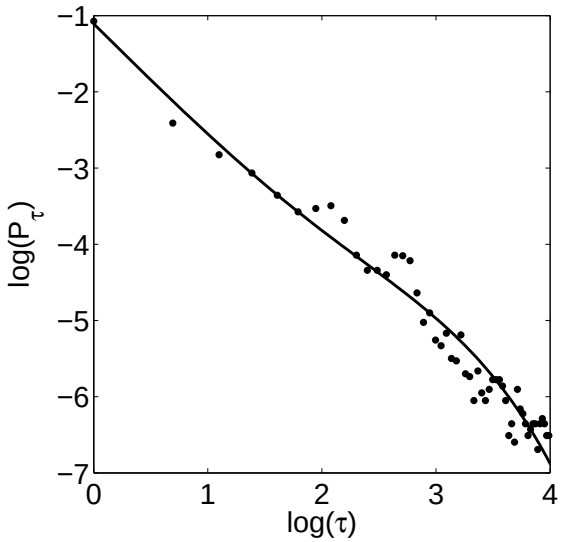

Figure 4.9: Scaling law for $\log \tau$ vs $\log P_\tau$ at $b = 0.308$ for system (4.1). τ is the mean time between bursts, P_τ is the distribution of τ. In this case $P_\tau \sim \alpha n^{-3/2} e^{-\beta n} + \gamma e^{-\delta n}$, where $n = 0.1\tau$, $\alpha = 0.3321$, $\beta = 0.0524$, $\gamma = 0.0156$, and $\delta = 0.0506$.

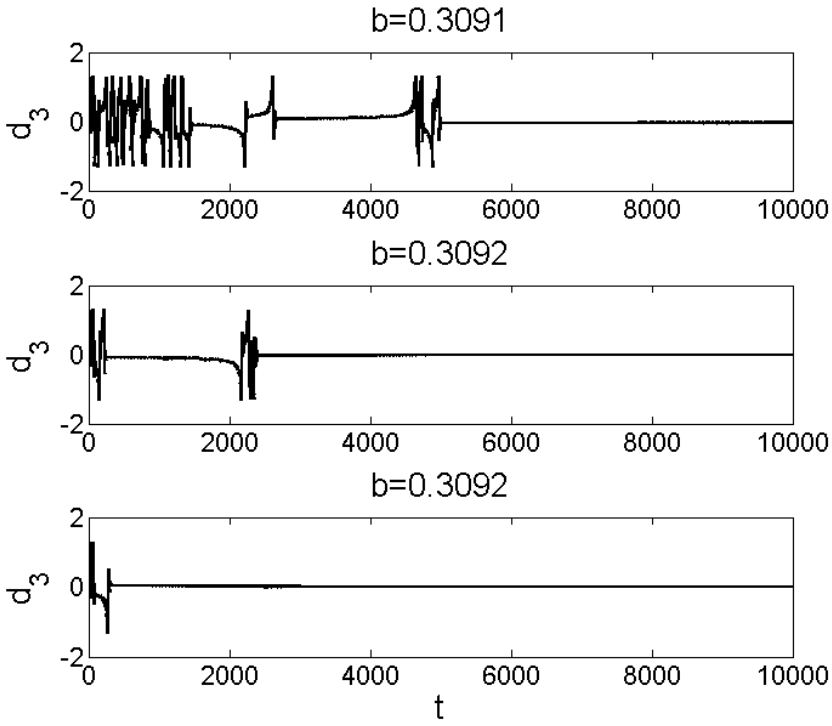

Figure 4.10: Time series of transient chaos in (4.1) following in-out intermittency in Figure 4.8.

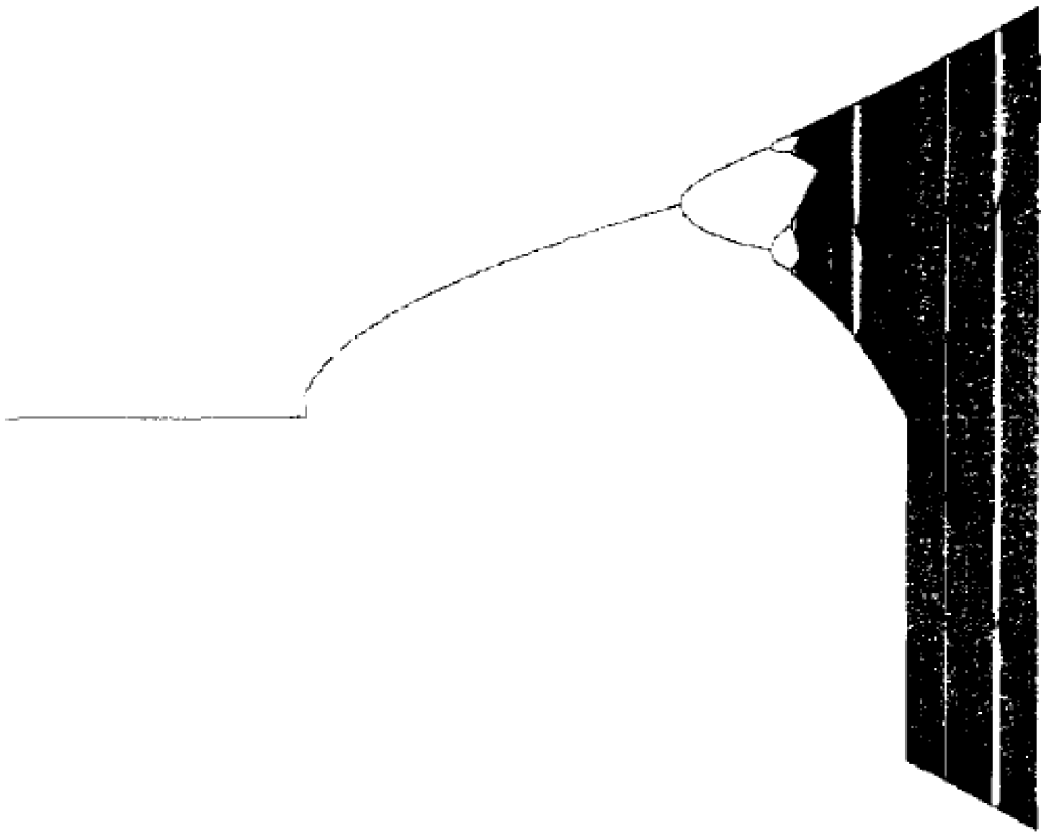

Figure 4.11: Bifurcation diagram of the odd-logistic equation (4.22), from [10]. Only one attractor is provided.

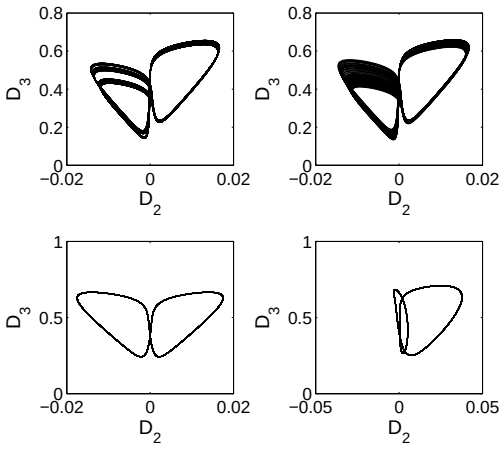

(a)

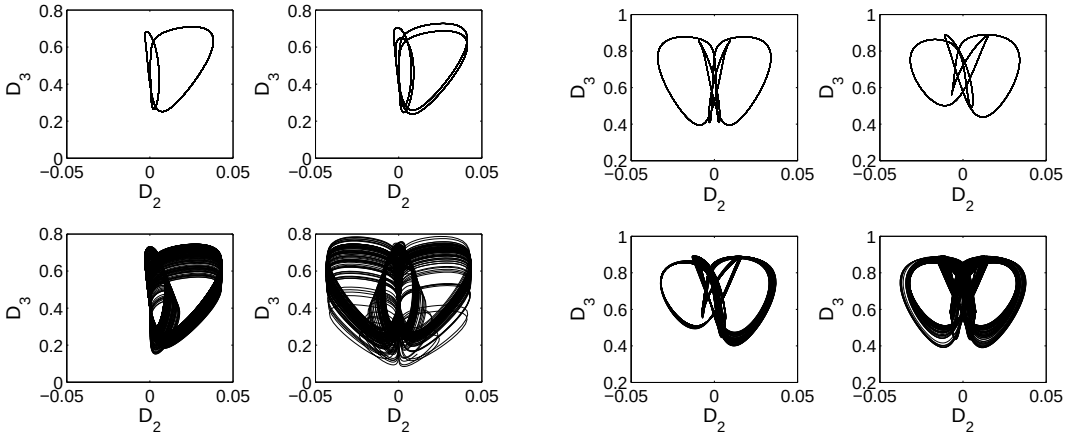

(b) (c)

Figure 4.12: Period doubling, symmetry increasing, symmetry decreasing, and bistability. (a): Phase portraits (D_2, D_3) for $b = 0$ (upper left), 0.004 (upper right), 0.0144 (lower left), and 0.0522 (lower right). (b): Phase portraits (D_2, D_3) for evolution of the asymmetric periodic orbit at $b = 0.053$ (upper left), 0.0569 (upper right), 0.0594 (lower left), and 0.0596 (lower right). (c): Phase portraits (D_2, D_3) for evolution of the symmetric periodic orbit at $b = 0.053$ (upper left), 0.0596 (upper right), 0.0609 (lower left), and 0.0611 (lower right).

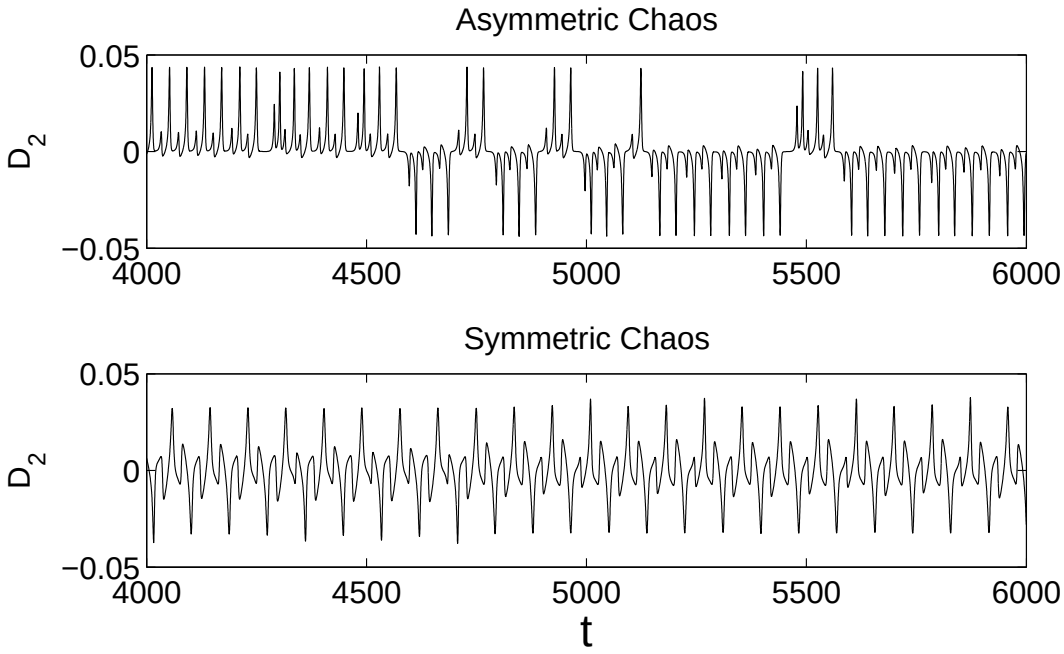

Figure 4.13: Bistability at $b = 0.0611$ for the perturbed normal form (4.1). Upper: time series of an intermittent switching for D_2-component for the asymmetric chaos. Lower: time series for symmetric chaos of D_2-component for symmetric chaos.

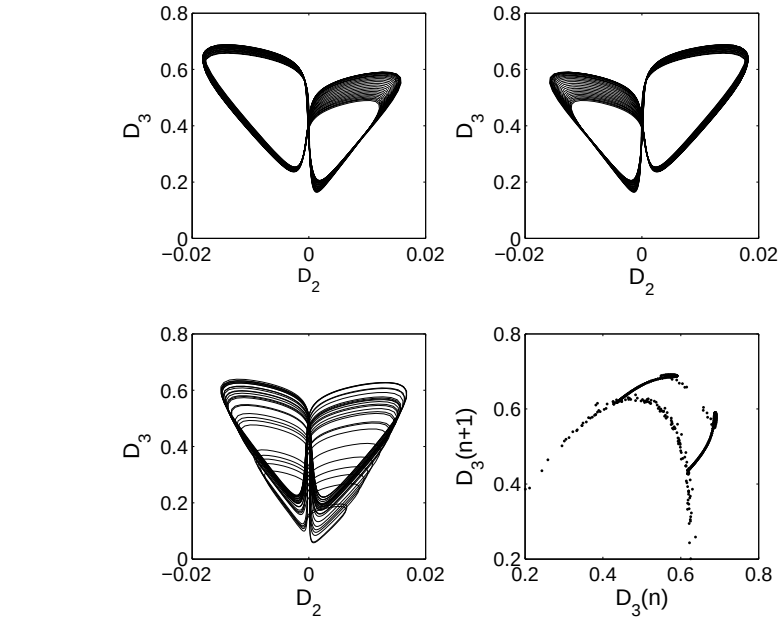

(a)

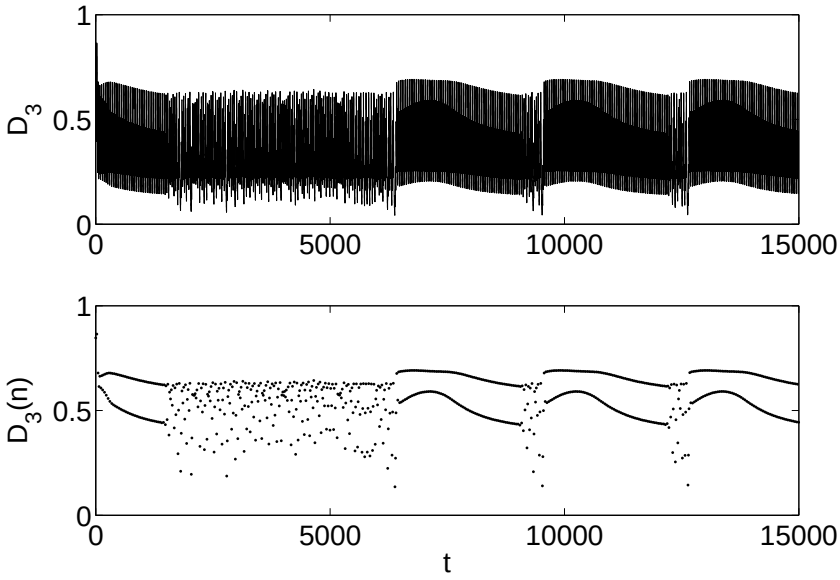

(b)

Figure 4.14: A new type of intermittency for the perturbed normal form (4.1) at $b = 0.0125$. (a): Intermittent behavior between a pair of conjugate asymmetric chaos (upper left and right) and symmetric chaos (lower left), and iterates of the Poincare map in $D_3(n+1)$ versus $D_3(n)$ (lower right). (b): Time Series of D_3 (upper) and the Poincare map $D_3(n)$ (lower).

Chapter 5

Conclusions

In summary, we study the nonlinear dynamics of the simulated spatiotemporal chaotic pattern (STC) from a system of Ginzburg Landau equations. The Ginzburg Landau system is used to study the weakly nonlinear stability of waves' amplitudes of nemtatic electroconvective patterns introduced in Section 1.2.2, and comparisons between predictions from the Ginzburg Landau system and the experimentally observed patterns are made in [21, 22, 42, 41]. In this dissertation two theoretical problems relating to this simulated STC are investigated, focusing on the symmetries and the dynamics of the associated symmetry-adapted variables.

The first problem, identification and characterization of this STC, is presented and explained in Chapter 3. The amplitudes of the pattern are represented in the form of Fourier expansion. It is found that four central modes form an invariant manifold (normal form), while other noncentral modes are equivalent to transverse variables to this invariant manifold. Even though a large number of degrees of freedom are involved in this STC, we can just focus on two variables based on symmetries and the dynamics of these modes, because the higher order modes in X-direction exhibit qualitatively similar dynamics as the first order modes in X-direction, and modes in Y-direction decay to zeros very quickly. One variable characterizes the dynamics

within the invariant manifold, the other describes the dynamics in the transverse direction of the invariant manifold, which is identified as in-out intermittency. The bursts of the transverse variable affect the dynamics of the central modes, and induce switches between a pair of symmetry conjugate chaotic sets in the normal form. A two-dimensional map is constructed to illustrate and analyze this process in [61].

The second problem focuses on how the noncentral modes, which are the transverse variables for the invariant manifold formed by four central modes, affect dynamics of the central modes [60]. We propose a perturbed normal form with a system parameter representing the magnitudes of transverse variables of the invariant manifold. A detailed study of symmetries and invariant subspaces in this system is provided, as well as the description of its complex dynamics, including symmetry increasing and breaking, various period doubling cascades, in-out intermittency, crisis-induced intermittency, chaotic transients, and so on. In a certain range of the system parameter dynamics of the normal form variables switches between a set of chaotic sets via crisis-induced intermittency, also called a symmetry increasing bifurcation. Therefore, we can conclude that the bursts of noncentral modes with certain magnitudes serve as a bridge to connect two symmetry conjugate chaotic sets in the normal form.

Further extensions of this work include an intensive numerical study of the Ginzburg Landau system to investigate where this STC in this dissertation is from, and what the before and after scenarios are. Due to the expensive computations, a clever method to chose nearby parameters and improvement of the numerical scheme need to be developed. Another exploration here is to examine the new type of intermittency described in Section 4.4.5. As far as we know, this intermittency has not been discussed yet in the literature. A simple low dimensional map based on continuous functions needs to be constructed to characterize this intermittency, through some statistical properties and the scaling power law.

Bibliography

[1] G. Ahlers. Experiments with rayleigh-béard convection. In I. Mutabazi, J. Wesfreid, and E. Guyon, editors, *Dynamics of Spatio-Temporal Cellular Structures*, volume 207, pages 67–94. Springer, 2006.

[2] I. S. Aranson and L. Kramer. The world of the complex Ginzburg-Landau equation. *Reviews of Modern Physics*, 74:99–143, 2002.

[3] P. Ashwin. Chaotic intermittency of patterns in symmetric systems. In M. Golubitsky, D. Luss, and S. Strogatz, editors, *Pattern Formation in Continuous and Coupled Systems, A Survey Volume*, volume 115, pages 11–24. Springer, IMA, 1999.

[4] P. Ashwin, J. Buescu, and I. Stewart. From attractor to chaotic saddle: a tale of transverse instability. *Nonlinearity*, 9:703–737, 1996.

[5] P. Ashwin, E. Covas, and R. Tavakol. Transverse instability for non-normal parameters. *Nonlinearity*, 12:563–577, 1999.

[6] E. Baranya, M. Dellnitzb, and M. Golubitsky. Detecting the symmetry of attractors. *Physica D*, 67:66–87, 1993.

[7] M. Bauer, S. Habip, D. R. He, and W. Martienssen. New type of intermittency in discontinuous maps. *Physical Review Letters*, 68:1625–1628, 1992.

[8] S. Chandrasekhar. *Hydrodynamic and Hydromagnetic Stability*. Dover Publications, 1981.

[9] P. Chossat and M. Golubitsky. Iterates of maps with symmetry. *SIAM Journal on Mathematical Analysis*, 19:1259–1270, 1988.

[10] P. Chossat and M. Golubitsky. Symmetry-increasing bifurcation of chaotic attractors. *Physica D*, 32:423–436, 1988.

[11] P. Chossat and R. Lauterbach. *Methods in Equivariant Bifurcations and Dynamical Systems*. World Scientific, 2000.

[12] E. Covas, R. Tavakol, P. Ashwin, A. Tworkowski, and J. M. Brooke. In-out intermittency in partial differential equation and ordinary differential equation models. *Chaos*, 11:404–409, 2001.

[13] C. Crebogi, E. Ott, F. Romeiras, and J. Yorke. Critical exponents for crisis-induced intermittency. *Physical Review A*, 36:5365–5380, 1987.

[14] C. Crebogi, E. Ott, and J. Yorke. Chaotic attractors in crisis. *Physical Review Letters*, 48:1507–1510, 1982.

[15] C. Crebogi, E. Ott, and J. Yorke. Crises, sudden changes in chaotic attractors, and transient chaos. *Physica D*, 7:181–200, 1983.

[16] C. Crebogi, E. Ott, and J. Yorke. Critical exponent of chaotic transients in nonlinear dynamical systems. *Physical Review Letters*, 57:1284–1287, 1986.

[17] M. Cross and P. Hohenberg. Pattern formation outside equilibrium. *Reviews of Modern Physics*, 65:851–1123, 1993.

[18] G. Dangelmayr. Complex dynamics near a Hopf bifurcation with symmetry: A parameter study. *Dynamical systems*, 25:1–38, 2010.

[19] G. Dangelmayr, G. Acharya, J. T. Gleeson, I. Oprea, and J. Ladd. Diagnosis of spatiotemporal chaos in wave-envelopes of a nematic electroconvection pattern. *Physical Review E*, 79:046215, 2009.

[20] G. Dangelmayr and E. Knobloch. Hopf bifurcation with broken circular symmetry. *Nonlinearity*, 4:399–427, 1991.

[21] G. Dangelmayr and I. Oprea. A Ginzburg Landau study of the weak electrolyte model for electroconvection. *Molecular Crystals & Liquid Crystals*, 413:2441, 2004.

[22] G. Dangelmayr and I. Oprea. Modulational stability of traveling waves in 2d anisotropic systems. *Journal of Nonlinear Science*, 18:1–56, 2008.

[23] G. Dangelmayr and M. Wegelin. Hopf bifurcations in anisotropic systems. In M. Golubitsky, D. Luss, and S. Strogatz, editors, *Pattern Formation in Continuous and Coupled Systems, A Survey Volume*, volume 115, pages 33–48. Springer, IMA, 1999.

[24] M. Dennin, G. Ahlers, and D. S. Cannell. Spatiotemporal chaos in electroconvection. *Science*, 272:388–390, 1996.

[25] M. Dennin, G. Ahlers, and D. S. Cannell. Patterns of electroconvection in a nematic liquid crystal. *Physical Review E*, 57:638649, 1998.

[26] M. Dennin, D. S. Cannel, and G. Ahlers. Patterns in electroconvection in the nematic liquid crystal I52. *Molecular Crystals & Liquid Crystals*, 261:337, 1995.

[27] M. J. Feigenbaum. Quantitative universality for a class of nonlinear transformations. *Journal of Statistical Physics*, 19:25, 1978.

[28] M. Golubitsky and I. Stewart. *The Symmetry Perspective*. Birkhauser, 2000.

[29] M. Golubitsky, I. Stewart, and D. G. Schaeffer. *Singularities and Groups in Bifurcation Theory, Volume II*. Springer, New York, 1988.

[30] J. F. Heagy, N. Platt, and S. M Hammel. Characterization of on-off intermittency. *Physical Review E*, 49:1140–1150, 1994.

[31] P. Hirschberg and E. Knobloch. Complex dynamics in the Hopf bifurcation with broken translation symmetry. *Physica D*, 90:56–78, 1996.

[32] Y. Hu, R. E. Ecke, and G. Ahlers. Time and length scales in rotating rayleigh-bénard convection. *Physical Review Letters*, 74:5040–5043, 1995.

[33] H. Ishii, H. Fujisaka, and M. Inoue. Breakdown of chaos symmetry and intermittency in the double-well potential system. *Physics Letters A*, 116:257–263, 1986.

[34] J. L. Kaplan and J. A. Yorke. Preturbulence: a regime observed in a fluid flow model of Lorenz. *Communications in Mathematical Physics*, 67:93–108, 1979.

[35] A. S. Landsberg and E. Knobloch. Oscillatory bifurcation with broken translation symmetry. *Physical Review E*, 53:3579–3600, 1996.

[36] E. N. Lorenz. Deterministic nonperiodic flow. *Journal of the Atmospheric Sciences*, 20:130–141, 1963.

[37] P. Manneville and Y. Pomeau. Intermittency and the Lorenz model. *Physics Letter*, 75A:1–2, 1979.

[38] R. M. May. Simple mathematical models with very complicated dynamics. *Nature*, 261:459–467, 1976.

[39] S. W. Morris, E. Bodenschatz, D. S. Cannell, and G. Ahlers. Spiral defect chaos in large aspect ratio rayleigh-bénard convection. *Physical Review Letters*, 71:2026–2029, 1993.

[40] T. Olson. *Hopf Bifurcation in Anisotropic Reaction Diffusion Systems Posed in Large Rectangles*. PhD thesis, Colorado State University, Department of Mathematics, 2010.

[41] I. Oprea and G. Dangelmayr. Dynamics and bifurcations in the weak electrolyte model for electroconvection of nematic liquid crystals: a Ginzburg Landau approach. *European Journal of Mechanics. - B/ Fluids*, 27(6):726–749, 2008.

[42] I. Oprea, I. Triandaf, G. Dangelmayr, and I. Schwartz. Quantitative and qualitative characterization of zigzag spatiotemporal chaos in a system of amplitude equations for nematic electroconvection. *Chaos*, 17:023101, 2007.

[43] E. Ott. *Chaos in Dynamical Systems*. Cambridge University Press, 2002.

[44] N. Platt, E. A. Spiegel, and C. Tresser. On-off intermittency: a mechanism for bursting. *Physical Review Letters*, 70:279–282, 1993.

[45] Y. Pomeau and P. Manneville. Intermittent transition to turbulence in dissipative dynamical systems. *Communications in Mathematical Physics*, 74:189–197, 1980.

[46] T. Price and T. Mullin. An experimental observation of a new type of intermittency. *Physica D*, 48:29–52, 1991.

[47] M. I. Rabinovich, A. B. Ezersky, and P. D. Weidman. *The Dynamics of Patterns*. World Scientific, 2000.

[48] R. C. Robinson. *An Introduction to Dynamical Systems*. Prentice Hall, 2004.

[49] M. Silber, H. Riecke, and L Kramer. Symmetry breaking hopf bifurcation in anisotropic systems. *Physica D*, 61:260, 1992.

[50] C. Sparrow. *The Lorenz Equations: Bifurcations, Chaos and Strange Attractors*. Springer-Verlag, 1986.

[51] J. W Swift. Hopf bifurcation with the symmetry of the square. *Nonlinearity*, 1:333–377, 1988.

[52] L. N. Trefethen. *Spectral Methods in MATLAB*. SIAM, 2001.

[53] M. Treiber and L. Kramer. Bipolar electrodiffusion model for electroconvection in nematics. *Molecular Crystals & Liquid Crystals*, 261:311, 1995.

[54] M. Treiber and L. Kramer. Coupled complex Ginzburg-Landau equations for the weak electrolyte model of electroconvection. *Physical Review E*, 58:1973, 1998.

[55] A. M. Turing. The chemical basis of morphogenesis. *Philosophical Transactions of the Royal Society of London. Series B, Biological Sciences*, 237:37–72, 1952.

[56] S. Venkataramani, T. M. Antonsen, E. Ott, and J. C Sommerer. On-off intermittency: power spectrum and fractal properties of time series. *Physica D*, 96:66–99, 1996.

[57] M. Wegelin. *Nichtlineare Dynamik raumzeitlicher Muster in hierarchischen Systemen*. PhD thesis, University of Tubingen, Department of Physics, 1993.

[58] T. Wildey. A pseudo-spectral method for the globally coupled Ginzburg Landau equations in 2D. Master's thesis, Colorado State University, Department of Mathematics, 2004.

[59] J. A. Yorke and E. D. Yorke. Metastable chaos: the transition to sustained chaotic behavior in the Lorenz model. *Journal of Statistical Physics*, 21:263, 1979.

[60] Y. Zou, D. Dangelmayr, and I. Oprea. Intermittency and chaos near Hopf bifurcation with broken $O(2) \times O(2)$ symmetry. *In preparation.*

[61] Y. Zou, D. Dangelmayr, and I. Oprea. Spatiotemporal chaos induced by in-out intermittency. *In preparation.*